Mineralium Deposita
https://doi.org/10.1007/s00126-019-00892-6

ARTICLE

The origin and evolution of V-rich, magnetite dominated Fe-Ti oxide mineralization; Northwest River Anorthosite, south-central Labrador, Canada

Anthony A. Valvasori[1] · John M. Hanchar[1] · Stephen J. Piercey[1] · Merline L. D. Fonkwe[2]

Received: 1 April 2019 / Accepted: 29 April 2019

Abstract

Zones of massive to semi-massive Fe-Ti oxide mineralization are present in the Northwest River Anorthosite, a ca. 1625-Ma Paleoproterozoic massif-type anorthosite located in the Grenville Province of south-central Labrador. The oxide mineralization is predominantly composed of coarse to very-coarse grained V-rich magnetite with less abundant coarse granular ilmenite and pleonaste that formed by exsolution from the primary, chemically impure magnetite; all observed oxide minerals have complex and abundant subsolidus reequilibration and exsolution textures. Using petrography, oxide mineral chemistry, whole-rock geochemistry, and oxide-anorthosite field relationships, a three-process model is proposed for the formation of the oxide mineralization: (1) late-stage magmatic crystallization of impure magnetite; (2) concentration of Fe-Ti oxides via solid-state remobilization; and (3) reequilibration during subsequent post-emplacement cooling and Grenvillian metamorphism. These subsolidus processes significantly modified the primary magmatic composition of the magnetite through exsolution and reequilibration. Results from in-situ magnetite EPMA and LA-ICPMS analyses were plotted on magnetite mineral chemical discrimination diagrams. The data display a wide spread and typically do not plot exclusively in the expected anorthosite-hosted Fe-Ti-V magnetite fields. This is most likely due to modification of magnetite chemistry during subsolidus cooling and reequilibration. As such, care must be taken when using magnetite discrimination diagrams for Fe-Ti-V deposits given the complex petrogenetic histories that magnetite within these types of deposits experience.

Keywords Magnetite · Fe-Ti oxide mineralization · Proterozoic massif-type anorthosite · Northwest River Anorthosite · Labrador

Introduction

Titanium and V are important industrial elements that are commonly extracted from the Fe-Ti oxide minerals magnetite (Fe_3O_4) and ilmenite ($FeTiO_3$) (Force 1991; Fabjan et al. 2001; Dill 2010). Ilmenite hosted by Proterozoic massif-type anorthosites is the only economic hard rock source of TiO_2, whereas vanadiferous magnetite, which is also found within massif-type anorthosite, is the most important mined sources of V (Force 1991; Kerr et al. 2013). The demand for V is predicted to sharply increase in the near future as V is a key component of the vanadium redox flow battery, which are the best-suited battery for grid storage associated with renewable energy generation from solar panels, hydroelectric dams, and windmills (Li et al. 2011). Correspondingly, understanding the processes of Ti-V genesis in massif-type anorthosites is critical for understanding potential Ti-V sources required for the emerging "green economy."

Currently, there are three active Fe-Ti oxide mines hosted in Proterozoic massif-type anorthosites including Lac Tio, Québec (Charlier et al. 2009), Tellnes, southwest Norway (Charlier et al. 2006), and Damiao, China (Chen et al. 2013). Other massif-type anorthosites are known to host large, but

Editorial handling: W. D. Maier

Electronic supplementary material The online version of this article (https://doi.org/10.1007/s00126-019-00892-6) contains supplementary material, which is available to authorized users.

✉ John M. Hanchar
jhanchar@mun.ca

[1] Department of Earth Sciences, Memorial University of Newfoundland, St. John's, NL A1B 3X5, Canada

[2] Labrador Institute of Memorial University of Newfoundland, P.O. Box 490, Station B, Happy Valley-Goose Bay, NL A0P 1E0, Canada

currently uneconomic, concentrations of Fe-Ti oxides including Suwalki (Poland) (Charlier et al. 2009), Lac St. Jean (Québec) (Morisset et al. 2010), and Marcy (New York State) (Ashwal 1982).

Proterozoic massif-type anorthosites were defined by Ashwal (2010) as temporally restricted (e.g., largely forming between ~ 1790 and ~ 1060 Ma) large composite igneous intrusive suites (i.e., massifs) dominantly composed of anorthositic rocks. Labrador contains several anorthosite massifs (Fig. 1), including the Nain Plutonic Suite, Mealy Mountains Intrusive Suite, Northwest River Anorthosite (NWRA), Harp Lake Intrusive Suite, Mistastin Massif, and the Atikonak River Complex (Ashwal 1993; Kerr et al. 2013).

During the exploration boom following the discovery of the Voisey's Bay Ni-Cu-Co deposit in 1994 (Ryan et al. 1995), numerous occurrences of Fe-Ti-V oxide mineralization were discovered (or reevaluated from earlier work) in various geologic settings throughout Labrador (e.g., Hinchey 1999; MacDonald 1999; Kerr et al. 2001, 2013; Dyke et al. 2004). Only a few of these occurrences, however, underwent follow-up evaluation and detailed descriptions, as exploration efforts largely targeted magmatic Ni-Cu-Co sulfide deposits (Kerr et al. 2013, and references therein). The oxide zones were considered to be of limited interest, unless associated with Ni-Cu-Co-(PGE)-bearing sulfide mineralization.

There is a general consensus that Fe-Ti oxide mineralization in Proterozoic massif-type anorthosites is broadly magmatic in origin (e.g., Ashwal 1982; Duchesne 1999; Dymek and Owens 2001; Charlier et al. 2015 and references therein). The trace and minor element composition of magnetite in anorthosite-hosted oxide deposits is thought to systematically vary with changes in factors, such as temperature of crystallization, as well as both the chemical composition and redox state of parental fluid or magma (Buddington and Lindsley 1964; Lindsley 1976; Dupuis and Beaudoin 2011; Dare et al. 2014; Knipping et al. 2015; Broughm et al. 2017); however, the understanding of Fe-Ti oxide genesis in massif-type anorthosites in Labrador and globally is still incompletely understood.

In light of the above-proposed models, this paper aims to evaluate the various controls on the formation of Fe-Ti oxides in Proterozoic anorthositic rocks in the NWRA in Labrador. The oxide mineralization within the NWRA can be used as an analogue to Fe-Ti oxide mineralization from massif-type anorthosites globally; thus, results from this study and our field and analytical approaches utilized within this manuscript can be used to better understand the formation and evolution of important Fe-Ti-V oxide deposits globally (Taner et al. 2000; Charlier et al. 2015).

The magnetite-rich nature of the Fe-Ti oxide mineralization and bona fide association with anorthosites allows us to evaluate empirical magnetite trace element discrimination diagrams derived from in-situ analyses of magnetite, which have been purported to discriminate hydrothermal and magmatic magnetite associated with various types of ore deposits. Two groups of discrimination diagrams exist: (1) those which differentiate hydrothermal and magmatic magnetite and (2) those which differentiate magnetite from various ore deposit types. Both types of discrimination diagrams have commonly been used and/or modified in a number of recent studies and also have questioned the accuracy, validity, and usefulness of these diagrams (e.g., Hu et al. 2014; Broughm et al. 2017; Wen et al. 2017).

Geologic background

Regional geology

The rocks of the eastern Grenville Province were assembled over ~ 700 Ma along the southeastern ancestral margin of the Laurentian craton; most of these rock units have experienced polyphase, high-grade metamorphism, and are gneisses (Li et al. 2008; Rivers 2015). The oldest exposed rocks within the eastern Grenville Province (> 1710 Ma; termed pre-Labradorian (Gower et al. 1992; Gower 1996; Gower and Krogh 2002; Rivers 2008) are migmatitic gneisses, the protoliths of which are interpreted to consist of sedimentary rocks that originally formed within a continental-margin basin.

The oldest components of the Labradorian terrane consist of a volcanic arc dated at ~ 1710 and ~ 1680 Ma (Gower and Krogh 2002). Arc magmatism ceased at ~ 1660 Ma likely due to arc accretion, which led to the continental crust becoming over-thickened leading to penetrative ductile deformation coupled with low-pressure metamorphism peaking at granulite facies (Gower 1996; Rivers 1997; Gower and Krogh 2002). Subsequent to the arc-accretion events, a pulse of bimodal mafic-anorthositic-monzogranitic magmatism was emplaced within the eastern Grenville Province (Rivers 1997; Gower and Krogh 2002). This magmatic pulse, dated at 1650–1625 Ma, includes the Mealy Mountains Intrusive Suite (MMIS) and the NWRA that presently lies within the Cape Caribou River Allochthon (CCRA) (Ashwal 1993; Gower and Krogh 2002). The MMIS and NWRA are interpreted to have formed as components of a single body and were subsequently tectonically separated (Krauss and Rivers 2004).

The Pinwarian orogeny (1520–1460 Ma) is interpreted to be associated with arc accretion and active margin shortening in an island arc or continental arc-margin setting (Gower and Krogh 2002; Augland et al. 2015). Rocks associated with the Pinwarian orogeny are dominantly felsic and intrude into older Labradorian crust (Gower and Krogh 2002; Gower et al. 2008). Deformation and metamorphism associated with

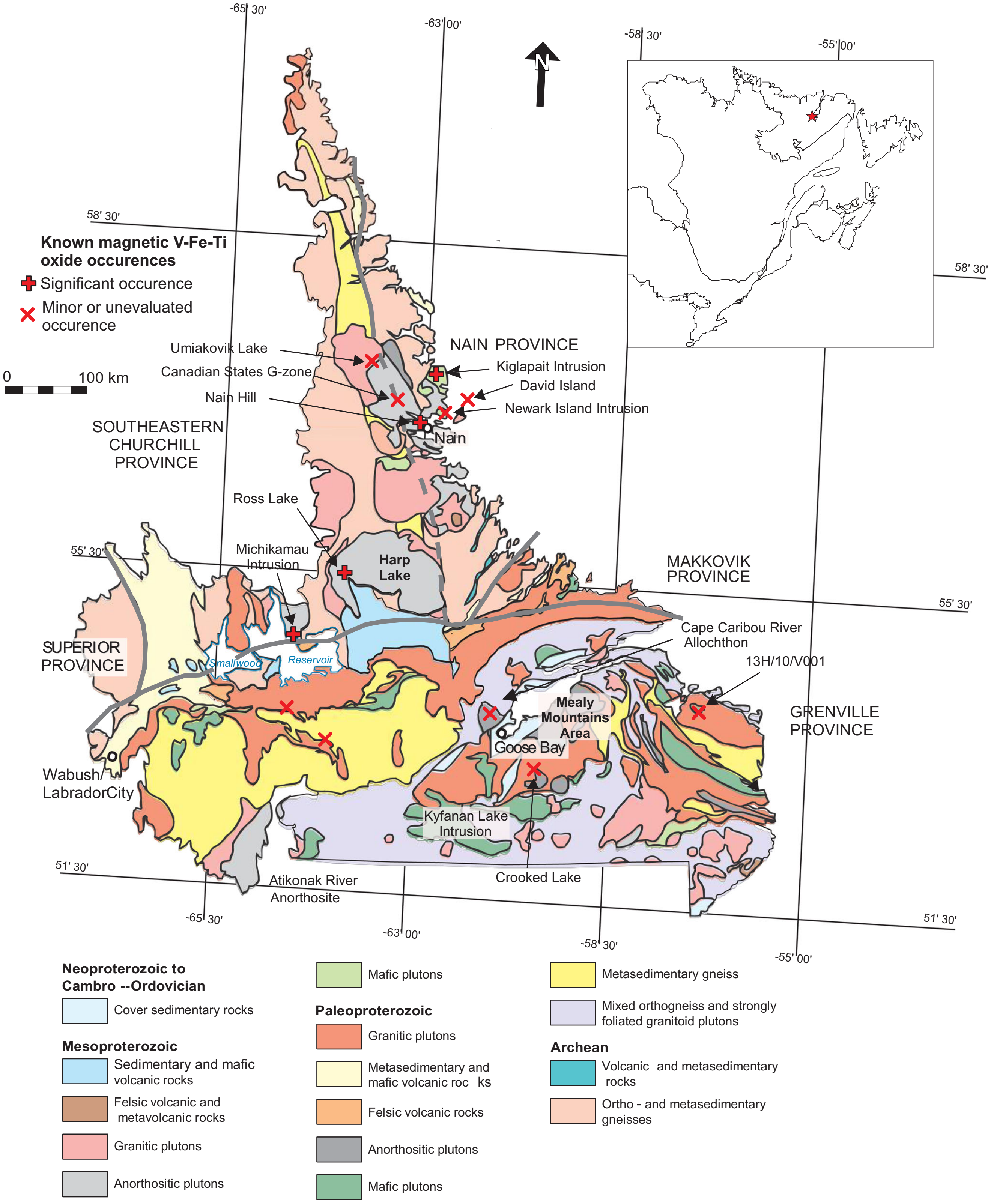

Fig. 1 Simplified geological map of Labrador showing locations of known magmatic Fe-Ti-V oxide mineralization (shown by red x and + symbols). The Cape Caribou River Allochthon is outlined by a black box (modified from Kerr et al. 2013)

the Pinwarian orogeny have been observed throughout the eastern Grenville Province (Augland et al. 2015).

Following the Pinwarian orogeny is the Elsonian orogeny (1460–1230 Ma). The Elsonian orogeny is interpreted to reflect the complex interactions between the subducting slab and the overriding Laurentian continental margin (Gower and Krogh 2002). The rocks of the Elsonian orogeny include the Michael-Shabogamo gabbroic dike swarm, as well as numerous anorthosite-mangerite-charnockite-granite (AMCG) suites, including the Nain Plutonic Suite (Rivers 1997; Gower and Krogh 2002).

The Grenvillian orogeny (1090 and 980 Ma) occurred due to the terminal continental collision between Laurentia and Amazonia, which led to extensive crustal thickening via thrust imbrication, as well as intense deformation and metamorphism (e.g., Rivers 1997; Li et al. 2008; Rivers et al. 2012; Rivers 2015 and references therein). Post-Grenvillian rifting, possibly associated with the opening of the early Paleozoic Iapetus Ocean, created a series of grabens in the Lake Melville area of Labrador, which now separate the CCRA from the MMIS (Fig. 1). The CCRA is believed to represent a portion of the MMIS that was separated during the formation of the Lake Melville rift as both the CCRA and the MMIS contain similar lithological assemblages (Wardle et al. 1990; Philippe et al. 1993; Krauss and Rivers 2004).

Geology of the study area

The CCRA (Fig. 2a) is a ~ 20–25-km wide lobate thrust sheet with an areal extent of ~ 500 km^2 that is dominantly composed of Paleoproterozoic AMCG rocks and also includes minor layered gabbroic monzonite, dioritic to granodioritic orthogneiss, amphibolite, mafic granulite, and minor metasedimentary gneiss (Wardle and Ash 1984, 1986; Ryan et al. 1982). Penetrative deformation in the CCRA is limited to the basal high-strain shear zone, whereas the uppermost units, including the NWRA, have undergone only static recrystallization (Krauss and Rivers 2004). The NWRA is an anorthositic body located at the structural top of the CCRA (Fig. 2a, b) (Bussy et al. 1995; Krauss and Rivers 2004).

The NWRA is a heterogeneous lithologic package composed primarily of anorthosite to gabbronoritic rocks that contain several coalesced anorthosite plutons, each with variable mafic components and textures (Krauss 2002). In general, plagioclase crystals in all coalesced plutons range from a few mm to 20 cm in length and are unaltered to weakly sericite altered. Despite the lack of penetrative deformation associated with thrusting, the NWRA shows evidence of static recrystallization, including the presence of garnet in gabbronorites, as well as recrystallization textures in plagioclase in the host anorthosite (Krauss 2002). The western edge of the NWRA is underlain by a large ~ 15 × 3-km aeromagnetic anomaly thought to correspond with oxide mineralization at depth. Fe-Ti oxide mineralization in the NWRA is dominated by magnetite.

Analytical methods

Field sampling

One hundred and sixty-four mineralized and unmineralized samples, representative of the anorthosite and gabbronorite host rocks observed in the field area and associated Fe-Ti oxide mineralization, were collected for this study. Sampling was done in a relatively small (~ 2 × 3 km) part of the intrusion where rocks above a large aeromagnetic anomaly outcropped. The field area is marked by a black box on Fig. 2a. Samples were subdivided into three categories: (1) massive to semi-massive oxide mineralization (50–100% oxide minerals); (2) disseminated oxide mineralization (10–49% oxide minerals); and (3) barren anorthosite host rocks (< 10 vol% oxide minerals). The samples were cleaned of any weathering rind by sawing and then cut into blocks for whole-rock major and trace element geochemical analyses and billets for polished thin sections.

Ninety-six samples showing representative oxide mineral abundances, as well as outcrop and hand-sample scale features, were sent to Actlabs for whole-rock major, minor, and trace element geochemical analysis, and 113 samples were sent to Vancouver Petrographics to be made into polished thin sections. The samples for polished thin sections and geochemical analysis were taken from the same rock material, with multiple thin sections made from selected coarse-grained massive to semi-massive oxide mineralized samples in order to obtain a more representative petrographic sample set. As a result, the number of thin sections is greater than the number of samples analyzed for major and trace elements.

Polished thin sections were examined using both reflected and transmitted light microscopy. Thin sections were organized based on both Fe-Ti oxide abundance (i.e., groups 1 and 2 above), outcrop textures observed during field work, and features observed in hand-sample, with petrographic description focusing on variations in mineralogy and exsolution textures within samples, between samples from the same mineralization style, and between samples from different mineralization styles. Representative grains and microtextures of magnetite, ilmenite, and pleonaste ($[Fe,Mg]Al_2O_4$) were analyzed using both electron probe microanalyzer (EPMA) and laser ablation inductively coupled plasma mass spectrometry (LA-ICPMS) where the grains were sufficiently coarse (i.e., when minerals analyzed were larger than 25 μm in their shortest axis).

Whole-rock geochemistry

The samples sent to Actlabs were powdered using a jaw crusher, disk mill, and tungsten-carbide shatter box and prepared for analysis using a lithium metaborate/tetraborate flux fusion followed by digestion in weak nitric acid. Samples were

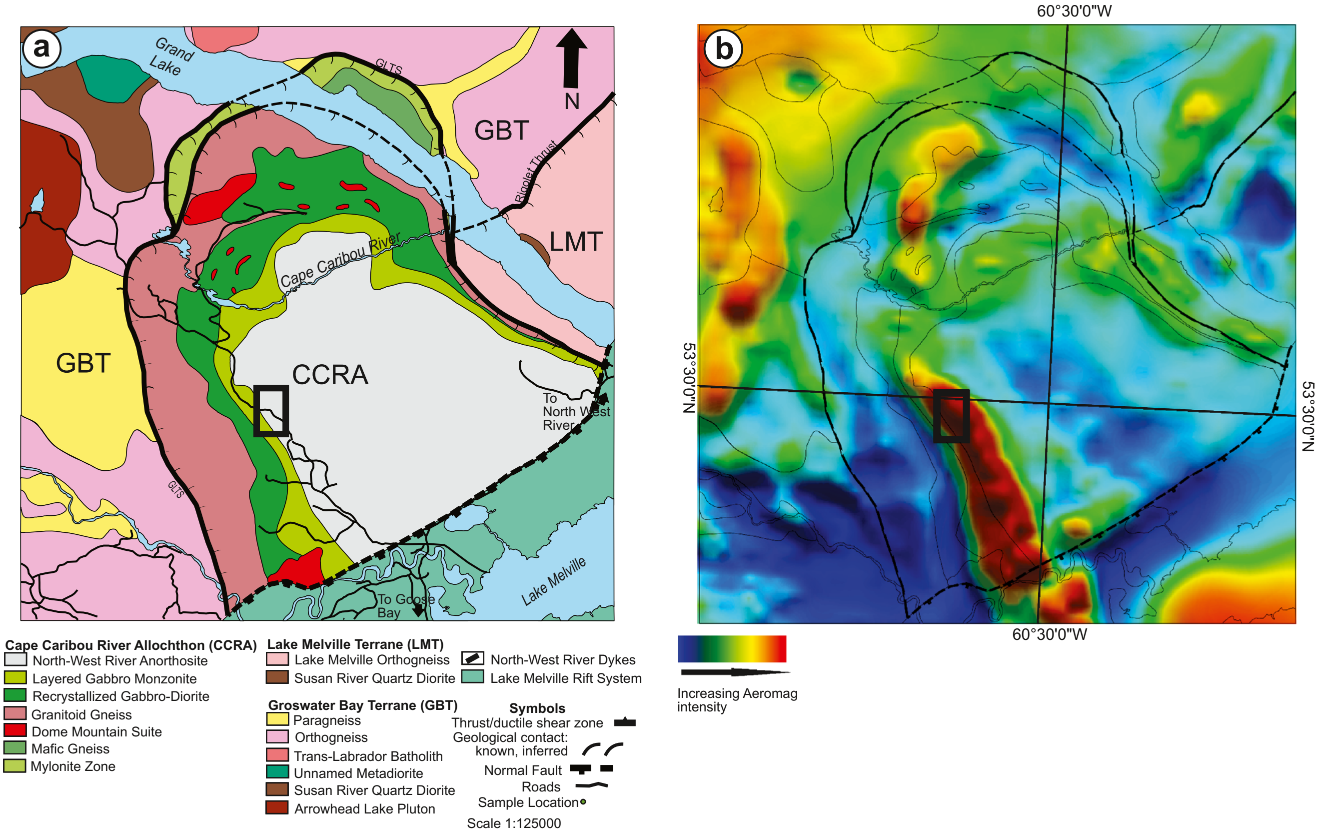

Fig. 2 **a** Geological map of the Cape Caribou River Allochthon showing the Northwest River Anorthosite in the center and surrounding rock units (modified from Krauss and Rivers 2004). **b** Regional aeromagnetic map (NL Geoscience Atlas) overlain by the unit boundaries of the rock units contained within Cape Caribou River Allochthon from the NL Geoscience Atlas. Note the relationship between the large aeromagnetic high and the contact between the Northwest River Anorthosite and basal layered monzonite. The field area for this study is outlined on both maps by a black box

analyzed using a combination of inductively coupled plasma mass spectrometry (ICPMS) and inductively coupled plasma optical emission spectroscopy (ICPOES), with 59 elements measured including major, minor, and trace elements using the Code 4LITHO+4B1(11+) Major Elements Fusion ICP(WRA)/Trace Elements Fusion ICP/MS(WRA4B2)/ Total Digestion ICP(TOTAL) analytical package. Duplicate samples were inserted every 10 analyses to ensure quality of analyses and reproducibility of results. The whole-rock lithogeochemistry data are presented in electronic Supplementary material (ESM) Table 1a.

Electron probe microanalyzer analyses

Electron probe analyses were done using wavelength dispersive spectroscopy (WDS) on nine representative thin sections selected based on field and petrographic observations (i.e., mineralization styles, textures, mineralogy). The analyses were done in order to determine if there are any compositional differences between similar textures of magnetite and ilmenite between different mineralization styles. The analyses were also intended to provide more chemical information on the various exsolution features observed in the oxide minerals. The EPMA analytical work was done at the Queens Facility for Isotope Research (QFIR) in the Department of Geological Sciences and Geological Engineering at Queens University, Kingston, Ontario. A JEOL JXA-8230 electron microprobe equipped with five WDS tunable spectrometers was used to determine the major and minor element compositions magnetite, ilmenite, and pleonaste (spinel) in a variety of microtextural settings from the nine polished thin sections. Although pleonaste was observed in every thin section, coarse grained pleonaste that could be analyzed by EPMA and LA-ICPMS was not present in enough of the samples to warrant discussion of the data or comparison to the other minerals in this study and will not be discussed further.

Point analyses were done using a focused beam with accelerating voltage of 15 kV and a beam current value of 50 nA. The concentrations of Si, Ti, Al, Cr, V, Fe, Mn, Mg, Ni, Ca, Cu, and K were determined in each analysis. Analyses with totals outside 100 ± 1.5 wt%, as well as analyses below the calculated detection limits, were discarded. For details on the EPMA instrumentation and diffracting crystals, X-ray lines, peak and background counting times, standards, and range of detection limits for each element analyzed, refer to ESM Tables 2a and 3a.

Electron probe WDS X-ray maps for Fe, Ti, V, Al, and Mg were made for eight representative textural-mineralogical features (e.g., grains of magnetite and ilmenite, as well as at contacts between magnetite and ilmenite in order to evaluate spatial chemical variations in the grains and to better understand exsolution and related textures) on six of the thin sections. An accelerating voltage of 15 kV, a sample current of 250 nA, and a dwell time of 200 ms per step were used for X-ray mapping. The step size ranged from 0.5 to 2 μm depending on the grain size of features of interest within the thin section.

For both point and X-ray map results, the Fe^{2+} and Fe^{3+} values in oxide minerals in this study were approximated using a method involving charge balance (B. Joy, personal communication). The charge balance recalculation method is thought to be accurate; however, errors can be introduced if the mineral is not charge balanced or contains vacancies in its crystal structure (Valvasori 2018). These errors have minimal effect on the interpretation of the data in this study.

LA-ICPMS analyses

LA-ICPMS analyses were done on the same thin sections and when possible on the same grains that were previously analyzed by EPMA. Like the EPMA analyses, the LA-ICPMS analyses were done to characterize the variation in minor and trace element compositions using a similar mineral and mineral texture approach as was used in the EPMA analysis (see above). Large-scale observable exsolution features were avoided in order to ensure that only the targeted oxide mineral was analyzed. However, many smaller-scale intergrowths could not be analyzed due to spatial limitations of the laser beam diameter used. LA-ICPMS analyses for ^{24}Mg, ^{25}Mg, ^{27}Al, ^{29}Si, ^{31}P, ^{34}S, ^{44}Ca, ^{45}Sc, ^{47}Ti, ^{51}V, ^{52}Cr, ^{55}Mn, ^{57}Fe, ^{59}Co, ^{60}Ni, ^{63}Cu, ^{66}Zn, ^{71}Ga, ^{74}Ge, ^{89}Y, ^{90}Zr, ^{93}Nb, ^{95}Mo, ^{118}Sn, ^{178}Hf, ^{181}Ta, ^{182}W, and ^{208}Pb were obtained on magnetite and ilmenite. However, depending on the target mineral, many of these elements were below detection limits and are therefore not discussed further.

The LA-ICPMS analyses were done at LabMaTer, University of Québec at Chicoutimi (UQaC), Chicoutimi, Québec, following the methods of Dare et al. (2014) and using an Agilent 7700× quadrupole ICP-MS interfaced to a Laurin technic S155 RESolution (193 nm) ArF excimer laser ablation system. Variations in isotopes of Ti, S, Ca, P, Al, and Cu in the oxide minerals were monitored throughout the analyses to ensure that the mineral analyzed was correctly identified and no mineral inclusions were included in the data integration. Instrument settings are presented in ESM Table 2a. Line analyses were done in this study in order to monitor elemental zonation as well as to homogenize microscopic exsolution microtextures. During line analyses, visible microtextures were avoided in order to minimize risk of contamination with unwanted material. The ICPMS was calibrated using reference material USGS GSD-1G (synthetic basaltic composition glass) using GeoReM preferred values (Jochum et al. 2005) and reduced using the Iolite version 2.5 software program (Paton et al. 2011). Values of Al, Ti, and $Fe_{(t)}$ from the EPMA analyses were used as internal standards for pleonaste (^{27}Al), ilmenite (^{47}Ti), and magnetite (^{57}Fe), respectively. Reference material GSE-1G (USGS) and G-probe 6 (BNV-1G, USGS) as well as in-house reference material BC-28 (a natural magnetite from the Bushveld Complex in South Africa) were used as secondary standards. LA-ICPMS results, which include average compositions and standard deviations from each mineralization style, are presented in ESM Tables 4a and 5a. However, in analyses where $n \leq 3$, standard deviations are not calculated.

Results

Field observations of styles of mineralization

Host rocks

The host rock to the oxide mineralization is the NWRA, a heterogeneous unit ranging in composition from anorthosite to gabbronorite, which is dominated by medium- to coarse-grained, white to light gray (and rarely lilac)-colored plagioclase crystals that range in diameter from < 1 to ~ 25 cm. Texturally, the plagioclase is granoblastic to prismatic and weakly saussuritized (i.e., altered to epidote group minerals), with the most intense alteration occurring nearest to the oxide-rich zones. Labradorescence (i.e., blue or green iridescence) is locally found associated with plagioclase throughout in the study area.

The coarse-grained ferromagnesian minerals observed in the host rocks of the NWRA include pyroxene (clinopyroxene > orthopyroxene), amphibole (hornblende and pargasite), and rare olivine. Ferromagnesian silicates occur as individual grains or as clusters of grains and are irregular in form, varying in size proportionally to the adjacent plagioclase grains with the largest plagioclase occurring adjacent to the largest ferromagnesian silicates (ranging from 5 mm to 20 cm). Ferromagnesian minerals occur in patches in the host anorthosite accounting between 0 and 70% of the total rock volume.

Fe-Ti oxide minerals are abundant in the NWRA and include massive to semi-massive (Fig. 3a, b) and disseminated mineralization. Oxide mineralization has sharp irregular contacts with host anorthosite (Fig. 3c–e). Zones of massive to semi-massive oxide mineralization are on the meter scale, discontinuous, and dwarfed in size by surrounding anorthosite.

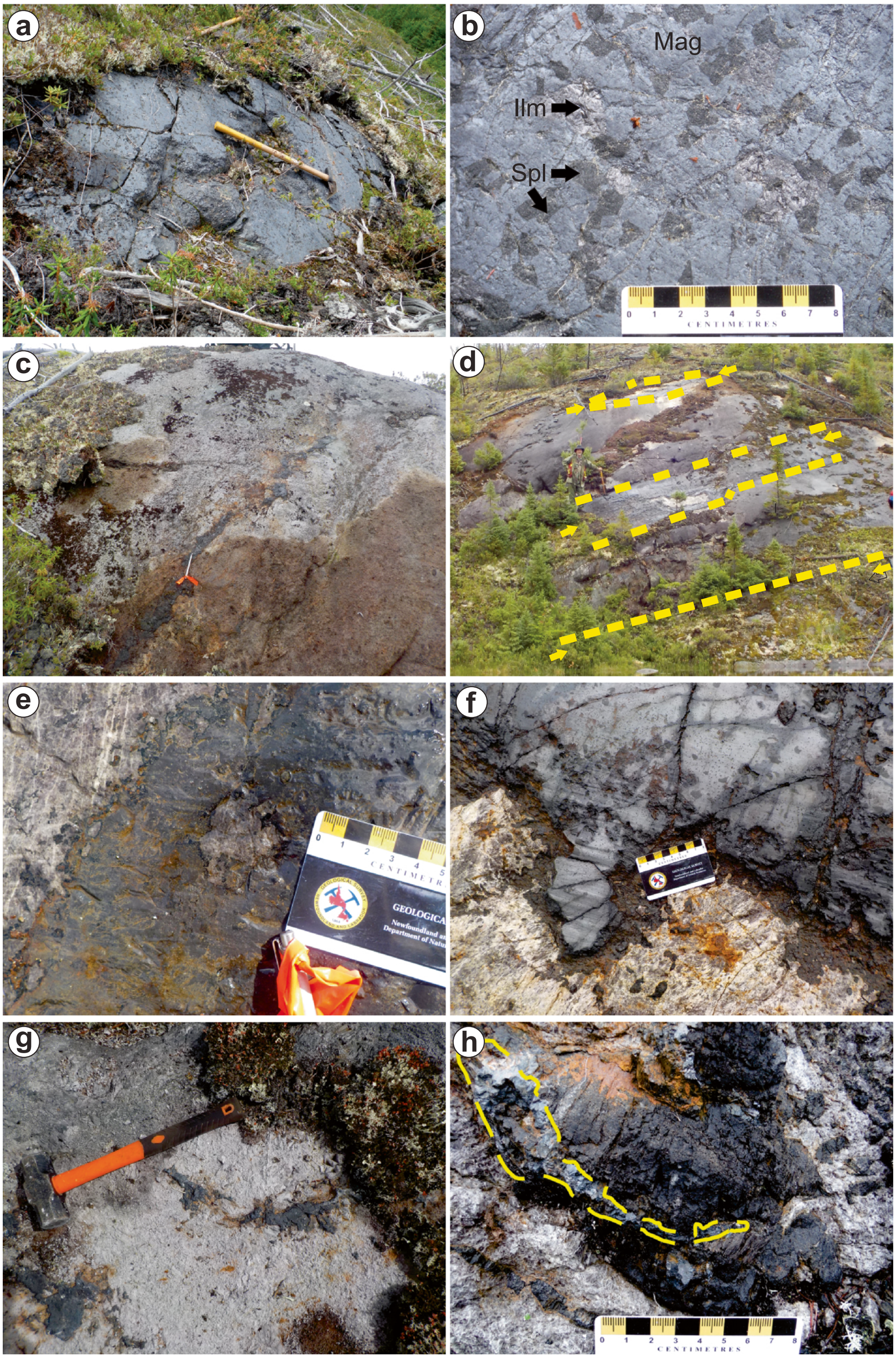

Fig. 3 Representative field photographs of Fe-Ti oxide mineralization. **a** Large pod of massive to semi-massive oxide mineralization (hammer is 75-cm long). **b** Close-up view of massive to semi-massive oxide mineralization. Note coarse-grained nature of oxide minerals. **c** Discontinuous, discordant vein of oxide mineralization tapering in diameter from bottom to top of the outcrop. **d** Large outcrop with three parallel bands of massive oxide mineralization as indicated by the arrows and yellow dashed lines, alternating with anorthosite layers. **e** Vein of oxide mineralization with sharp irregular contact with host anorthosite and a small inclusion of host anorthosite. **f** Close-up of irregular contact between band of oxide mineralization and host anorthosite, perhaps a density-driven structure. **g** Anorthosite hosted disseminated oxide that is anhedral. **h** Oxide mineralization (outlined in yellow) crosscutting and partially rimming an orthopyroxene megacryst. Abbreviations: Mag—magnetite; Ilm—ilmenite; Spl—spinel (pleonaste)

Massive to semi-massive oxide mineralization

Massive to semi-massive oxide mineralization (50–100 vol% oxide minerals at the outcrop scale) occurs in three styles: (1) oxide-rich pods, (2) oxide-rich veins, and (3) alternating bands of oxide mineralization and host anorthosite (Fig. 3). Oxide-rich pods are the most commonly observed style of massive to semi-massive oxide mineralization within the field area (Fig. 3a, b). They vary in size with the largest observed pod measured at more than 8 m × 4.5 m at surface, with most ranging from 1 to 2 m in diameter. Although the pods are generally of equant dimensions, they can locally be lenticular to elongate in shape.

Veins of oxide mineralization are rarely observed in the field area. However, where present, they are typically 3–30 cm in width and have sharp contacts with the host anorthosite (Fig. 3c, e). These veins vary in width along strike and can be discontinuous over tens of meters (Fig. 3c). Oxide-rich veins locally contain small inclusions of host anorthosite (Fig. 3e).

Alternating oxide and anorthosite bands were observed in only two localities where a maximum of three parallel oxide bands occur in sequence. When observed, bands of oxide mineralization occur as two or more broadly parallel bands of continuous massive oxide that are > 30-cm wide and alternate with variably-sized, but generally thicker bands of anorthosite (Fig. 3c). Contacts between the oxide bands and the host anorthosite are sharp and irregular (Fig. 3c, f).

Although individual oxide bands appear similar to vein occurrences, they differ in several distinct ways: (1) the contacts between oxide bands and anorthositic rocks are characterized by thinner bands of hydrous minerals than observed in vein-anorthosite contacts; (2) the oxide bands are more clearly defined and traceable along strike; (3) the larger oxide bands locally contain large anorthosite inclusions; (4) the oxide abundance varies within bands, from massive to semi-massive; and (5) veins occur as single units, whereas bands occur in series.

For the purpose of this study, massive to semi-massive oxide mineralization styles were defined solely using their surface expression. As such, it is unclear if there is continuity between various mineralization styles at depth.

Regardless of field context, oxide minerals in massive to semi-massive oxide mineralization are coarse-grained (0.5–3 cm) (Fig. 3a, b) and composed of (in decreasing order of abundance): magnetite, ilmenite, and pleonaste. Aside from the oxide minerals, plagioclase, orthopyroxene, pyrrhotite, pyrite, and chalcopyrite are also present in hand-sample and thin section. Texturally, plagioclase and orthopyroxene occur as resorbed grains or in monomineralic clusters of grains with a dark rim of amphibole and biotite present at the contact between both orthopyroxene and plagioclase and surrounding oxide minerals. Contacts between massive to semi-massive oxide mineralization and host rock are sharp and irregular and commonly show a mm- to cm-scale rim of hydrous minerals (e.g., biotite, pargasite, hornblende) at the oxide-silicate contact (Fig. 3e, f).

Disseminated oxide mineralization

Disseminated oxide mineralization (~ 10–49% of the mineralized rocks are composed of oxide minerals on the outcrop scale) is the most commonly observed mineralization style in the field area. There are two subtypes of disseminated oxide mineralization present: (1) disseminated oxide mineralization in the host anorthosite (Fig. 3g) and (2) disseminated oxide mineralization associated with pyroxene (Fig. 3h).

Oxide grains associated with pyroxene are variable in size and generally form partial rims around pyroxene or occur as cross-cutting features (Fig. 3h). In contrast, disseminated oxide mineralization hosted by anorthosite tends to be heterogeneously distributed with oxide grains interstitial to plagioclase grains. In both cases, there are polymineralic rims of biotite and amphibole developed around the oxides, ranging from ~ 3 mm to 2 cm in width.

Disseminated oxide mineralization observed in this study is not composed of small grains of oxide minerals that are evenly distributed throughout the host rock. Rather, it consists of relatively coarse-grained, irregular-shaped aggregates of Fe-Ti oxide minerals that are widely dispersed throughout the host rock.

Petrography

Host-rock to the Fe-Ti oxide mineralization

The host rocks to Fe-Ti oxide mineralization are anorthosite to gabbronorite, which have similar mineral assemblages. Silicate minerals include plagioclase, clinopyroxene, biotite, and pargasite, with rare orthopyroxene, olivine, and apatite. Plagioclase is granoblastic in texture, and the crystals range in size from 1 mm to 5 cm in diameter. Clinopyroxene is the most abundant ferromagnesian mineral in the host rocks and is anhedral and commonly occurs in monomineralic clusters. Coronas composed of amphiboles (Fe-Mg amphibole, pargasite, and hornblende) and biotite (Butt 2000) are present at contacts between plagioclase and oxide mineralization.

Massive to semi-massive oxide mineralization

Regardless of the mineralization style, the massive to semi-massive oxide mineralization is dominated by magnetite (~ 50–70%), ilmenite (~ 20–35%), and pleonaste (~ 15–20%). Two textural varieties of oxide mineralization are present in the NWRA: coarse-grained and granoblastic. Coarse-grained magnetite (Fig. 4a) is typically ~ 1 mm–4 cm in diameter and subhedral, whereas granoblastic magnetite is finer-grained (1–3 mm) (Fig. 4b). The ilmenite associated with coarse-grained magnetite ranges in size from ~ 6 mm to 2 cm and is typically subhedral to anhedral. Pleonaste is subhedral and commonly spatially associated with ilmenite grains of similar size or fine-grained and within ilmenite at the ilmenite-magnetite contact (Fig. 4c–e). Contacts between oxide minerals are sharp and irregular, commonly with pleonaste occurring at the contact between magnetite and ilmenite, or within ilmenite adjacent to magnetite (Fig. 4d).

Massive to semi-massive oxide mineralization contains numerous silicate minerals, including plagioclase, orthopyroxene, and clusters of pargasite ± hornblende ± biotite ± garnet.

Oxide mineralization displays a range of complex exsolution textures in magnetite, ilmenite, and pleonaste, which are defined in Valvasori (2018). Magnetite contains complex and abundant exsolutions of pleonaste, and ilmenite. Coarse-grained granular pleonaste is commonly associated with composite ilmenite of similar grain size (Fig. 4e). Coarse-grained ilmenite contains lamellae of magnetite with variable amounts of pleonaste (Fig. 4f), as well as hematite lenses. Coarse pleonaste commonly contains lenses of magnetite (Fig. 4c).

Disseminated oxide mineralization

Disseminated oxide mineralization is hosted in both anorthosite and gabbronoritic anorthosite, and is irregular in form, occurring as clustered aggregates that range in size from 1 mm to 5 cm, with individual oxide minerals ~ 0.5 mm to 2 cm in diameter. Where hosted in anorthosite, the oxide minerals occur interstitial to plagioclase (Fig. 4g), whereas when hosted by gabbronorite, the oxide minerals are typically spatially associated with pyroxene, and the oxide minerals commonly form as partial rims on clinopyroxene (Fig. 4h). Disseminated mineralization (Fig. 4g) has similar mineralogy and exsolution features as massive to semi-massive mineralization; however, exsolution features are finer grained and coarse-grained pleonaste granules are not observed.

Whole-rock geochemistry

Geochemical data for host rocks, disseminated, and semi-massive to massive mineralization are presented in Fig. 5 and ESM Table 1a. Unmineralized host rocks are dominantly composed of SiO_2, Al_2O_3, CaO, and alkalis (ESM Table 1a; Fig. 6) and have relatively similar major and trace element compositions. However, samples containing ferromagnesian silicate minerals, including the barren gabbronorite and the olivine-bearing anorthosite, have higher $FeO_{(t)}$, MgO, Co, Ni, and Zn content and lower abundances of SiO_2, Al_2O_3, alkalis, Sr, and Ba compared with the anorthosite (Fig. 5).

Samples of orthopyroxene-rich ($n = 8$) and orthopyroxene-poor ($n = 21$) massive to semi-massive oxide mineralization are predominantly composed of $FeO_{(t)}$ and TiO_2 with abundant V and highly variable SiO_2, Al_2O_3, and alkalis and share similar ranges of most other major, minor, and trace elements. Exceptions include relative enrichment in Mg, Cr, Co, and Ni in the orthopyroxene-bearing samples, which are coupled with lower Al, Sr, and Ba contents relative to samples without orthopyroxene (Fig. 5).

Geochemical correlations

A correlation matrix for whole-rock analyses illustrates two trends (Fig. 6): (1) strong to very strong positive correlations are present between elements compatible in Fe-Ti oxide minerals, including Fe, Ti, Mn, V, Cr, Co, Ni, Zn, Ga, and Sc, and between elements that are compatible within plagioclase including Si, Ca, Na, K, Al, Ba, and Sr; and (2) there are strong negative correlations between elements associated with Fe-Ti oxide minerals vs. those compatible in plagioclase and vice-versa. LOI (loss on ignition) values are strongly correlated with Si content. Phosphorus, reflecting the apatite content, is weakly negatively correlated with elements associated with Fe-Ti oxide minerals. Magnesium contents are not correlated with either SiO_2 or $FeO_{(t)}$ and are likely controlled by the presence of ferromagnesian silicates like orthopyroxene, clinopyroxene, or rarely olivine.

Binary variation diagrams were generated using SiO_2 and $FeO_{(t)}$ as variation indices (Fig. 5). Each figure contains gray ellipses labeled with a mineral abbreviation, which represents the compositional range of that mineral. When the compositional range of that mineral plots outside of the bounds of the graph, the direction of its compositional range is denoted by an arrow. Aside from showing some of the aforementioned correlations, these diagrams show that two distinct clusters of data are present: (1) one cluster is rich in elements that are associated with Fe-Ti oxide minerals and poor in elements that are associated with plagioclase; and (2) the other is enriched in elements that are associated with plagioclase and poor in elements that are associated with Fe-Ti oxide minerals. With the exception of a few intermediate samples, the gap in these clusters spans between ~ 20–45-wt% SiO_2 content and ~ 20–45-wt% $FeO_{(t)}$. The nature of this gap is unclear; however, it may be associated with the lack of observed semi-massive oxide mineralization, or a sampling bias due to the coarse-grained nature of the rocks within the study area.

In-situ analyses

Electron probe and LA-ICPMS analyses were done on magnetite and ilmenite from all mineralization styles. Regardless of mineralization style, all magnetite that was analyzed contains impurities, including Ti, Al, Cr, Mg, and V (ESM Table 4a). Likewise, ilmenite from all mineralization styles contains minor impurities including V, Mg, and Mn (ESM Table 5a).

Magnetite analyses from the NWRA show strong positive correlations between Fe^{2+} and Ti, Al, Mg, and Mn and are strongly negatively correlated with Fe^{3+} in all analyses (Fig. 7). This relationship geochemically confirms the presence of pleonaste and ilmenite exsolution in magnetite that is observed in thin section. In contrast, the Cr and V contents are

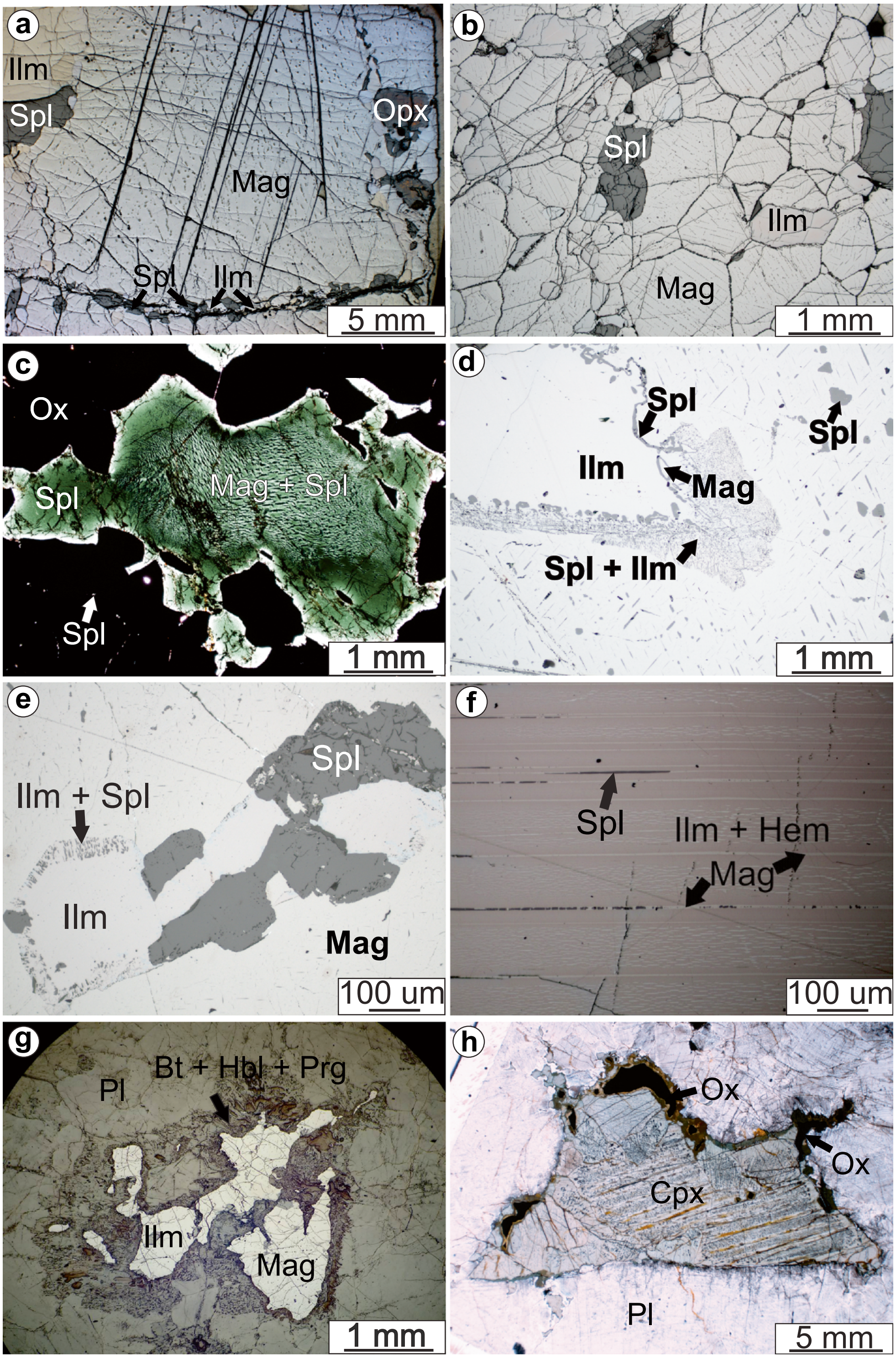

similar in all coarse-grained magnetite and are not correlated to any other elements, suggesting that Cr and V are largely unaffected by exsolution and reequilibration during cooling and metamorphism. Like in magnetite, ilmenite analyses show a strong positive correlation between Ti and Fe^{2+} coupled with a strong negative correlation between Fe^{2+} and Fe^{3+} in all ilmenite analyses.

Wavelength dispersive spectroscopy (WDS) X-ray maps of oxide grains

Maps containing representative results are shown in Fig. 8. In general, similar chemical features are observed for each element in all of the X-ray maps: magnetite is relatively homogeneous with a few exceptions.

◀ **Fig. 4** Representative photomicrographs of Fe-Ti oxide mineralization. **a** Large grain of magnetite containing abundant exsolution microtextures including large lamellae of ilmenite and pleonaste as well as fine-grained granules of pleonaste, which occur abundantly throughout magnetite grain. Note granoblastic zone of pleonaste and ilmenite rimming magnetite. **b** Granoblastic zone of oxide mineralization. **c** Large grain of pleonaste in massive to semi-massive oxide mineralization. Magnetite lamellae are present in the core of the grain and diminish towards the Fe-Ti oxide minerals. **d** Composite ilmenite in magnetite. Contact between Fe-Ti oxide minerals either ilmenite dotted with pleonaste microcrystals, or irregular with a rim of pleonaste. Note abundant pleonaste exsolution in magnetite. **e** Association of composite ilmenite and pleonaste in magnetite. **f** Close-up photomicrograph of exsolution microtextures in ilmenite including magnetite and pleonaste lamellae and hematite lenses. Hematite content depletes approaching magnetite lamellae. **g** Typical disseminated oxide mineralization hosted in anorthosite. Note irregular nature and clustered habit. **h** Coarse grained clinopyroxene partially rimmed by oxide mineralization. Abbreviations: Mag—magnetite; Ilm—ilmenite; Spl—spinel (pleonaste); Opx—orthopyroxene; Cpx—clinopyroxene; Pl—plagioclase; Ox—oxide minerals; Prg—pargasite; Bt—biotite; Hbl—hornblende

Ilmenite grains that are adjacent to magnetite typically display a narrow rim enriched in Ti, coupled with a depletion in Fe (Fig. 8a–c). Locally, this zone contains irregular regions enriched in Mg and Al, which correspond to pleonaste observed in thin section.

Two other exsolution textures within ilmenite are illustrated clearly in the WDS X-ray maps. The first shares a textural form with hematite lenses identified petrographically and is chemically defined by an enrichment in Fe and V coupled with a depletion in Ti (Fig. 8c, d). In general, the hematite lenses are most abundant in the cores of ilmenite grains and gradationally diminish in abundance approaching the contacts between ilmenite and magnetite. Within the largest of these hematite lenses, lamellae enriched in Ti are present (Fig. 8c). The second intergrowth texture is composed of lamellar features that are enriched in Al and Mg and depleted in Fe compared with the host ilmenite. These lamellae correspond with pleonaste observed in thin section. Surrounding these lamellae are zones slightly enriched in Ti and slightly depleted in Fe.

Discussion

Evaluating empirical magnetite mineral chemistry discrimination diagrams

Magnetite is a critical mineral in ores of numerous mineral deposit types, including iron oxide Cu-Au (IOCG), porphyry Cu-Au, magmatic Cu-Ni-PGE, and massif anorthosite Ti-V deposits (e.g., Charlier and Grove 2012; Dare et al. 2012; Hitzman et al. 1992; Nadoll et al. 2015). Because of this, understanding the origin of magnetite can provide critical insight into the origin of specific mineral deposits. The trace and minor element composition of magnetite is thought to systematically vary with changes in temperature of crystallization, as well as the chemical composition and redox state of parental fluid or magma during magnetite crystallization; thus, understanding magnetite origin provides insight into not only the physicochemical conditions of magnetite formation but also the associated mineral deposit it is associated with (Buddington and Lindsley 1964; Lindsley 1976; Dupuis and Beaudoin 2011; Dare et al. 2014; Knipping et al. 2015). Based on this principle, several empirical magnetite discrimination diagrams have been proposed with fields derived from in-situ analyses of magnetite from various types of ore deposits.

Dupuis and Beaudoin (2011) utilized Ca + Al + Mn (wt%) vs. Ti + V (wt%) and Ni/(Cr + Mn) vs. Ti + V (Fig. 9) diagrams to discriminate magnetite from various geologic environments. Our results from bona fide Proterozoic massif-type anorthosite mineralization illustrate that approximately half of the data from the NRWA mineralization plot in the Fe-Ti, V field, whereas other samples plot between the porphyry and Kiruna-type fields (Fig. 9a). Similarly, in Ni/(Cr + Mn)-Ti + V space, the data are spread across the Fe-Ti, V oxide, porphyry, and skarn fields. Notable, however, is that the samples with the highest Ti contents consistently plot correctly within the Fe-Ti, V oxide field. This illustrates that there are potential problems with these diagrams in discriminating magnetite from massif-type anorthosite environments for samples that have magnetite that does not contain elevated Ti content.

Knipping et al. (2015) proposed an empirical discrimination diagram for discriminating magmatic and hydrothermal magnetite using Ti and V (ppm) contents (Fig. 10a). The results from the NRWA also illustrate that this diagram is ineffective as the majority of coarse-grained magnetite data plot above the defined discrimination fields. The data points for all analyzed coarse-grained magnetite have similar V contents, with the exception of analyses from clinopyroxene-associated disseminated oxide mineralization, which have slightly lower V contents than other analyzed samples in this study. The Ti content of the NWRA magnetite is much more variable, however, as samples with the highest Ti contents plot barely within the magmatic magnetite field (Fig. 10a).

Dare et al. (2014) also presented an empirical discrimination diagram to discriminate between magmatic and hydrothermal magnetite. The diagram uses the Ni/Cr and Ti content (Fig. 10b), and results from this study illustrate that this diagram appears to be effective for discriminating magmatic from hydrothermal magnetite.

With the exception of the Dare et al. (2014) diagram, the aforementioned discrimination diagrams are generally ineffective in discriminating magnetite data from Proterozoic massif-type anorthosite-hosted Fe-Ti-V mineralization. There are two possible reasons for this. First, Ti and Al are used in most discrimination diagrams, and the Ti and Al contents in magnetite are known to be extensively modified by exsolution of ilmenite and pleonaste, respectively (Buddington and

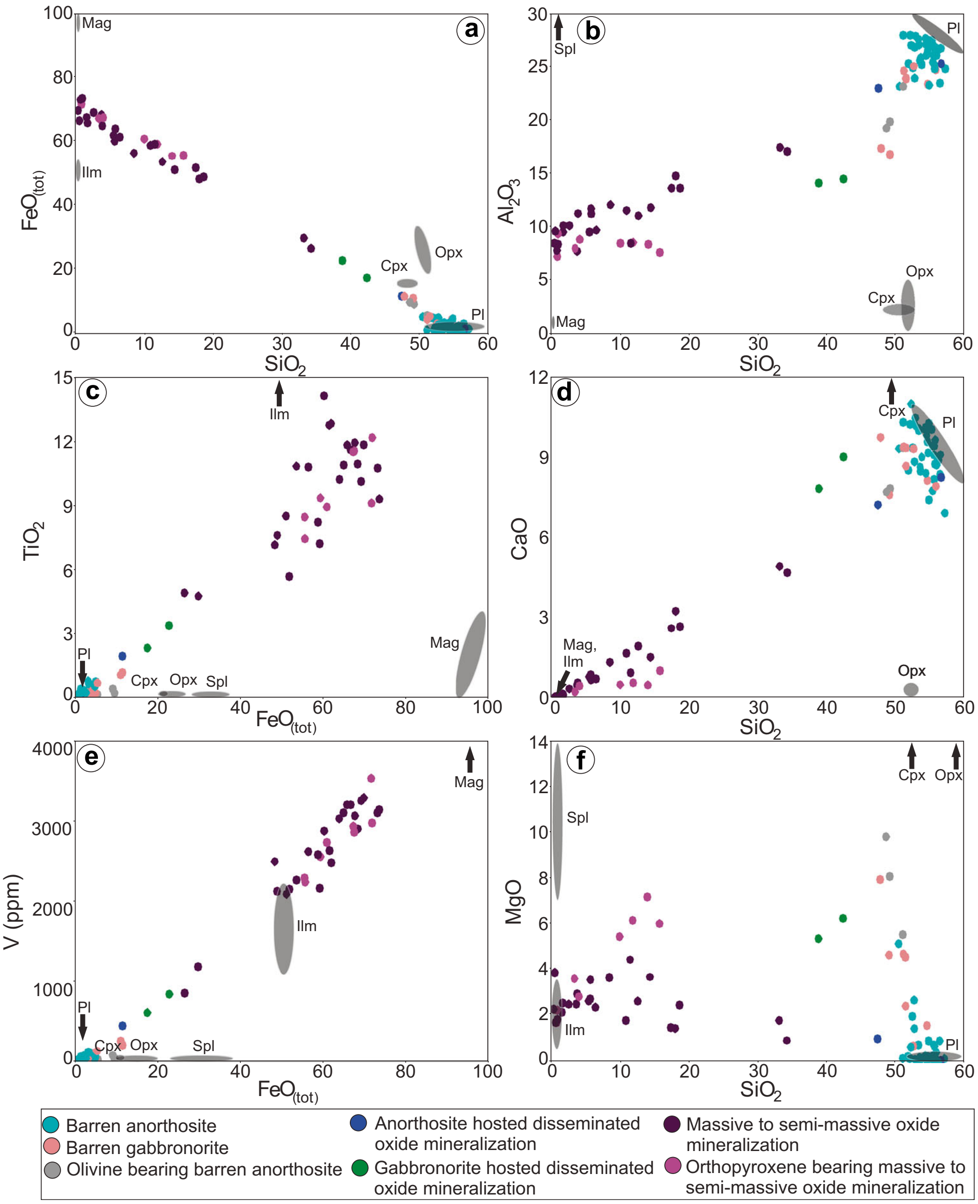

Fig. 5 Binary variation diagrams of whole-rock geochemical analyses from the Northwest River Anorthosite (NWRA). Axis units are in wt% except for V, which is in ppm. Compositional ranges of minerals observed are represented by ellipses or indicated by an arrow when beyond the bounds of the graph. Silicate mineral ellipses are based on the typical compositional ranges of those minerals in labradorite-type Proterozoic massif-type anorthosites Charlier et al. (2009). Pl = plagioclase, Opx = orthopyroxene, Cpx = clinopyroxene, Mag = magnetite, Ilm = ilmenite, and Spl = spinel (pleonaste) spinel

Lindsley 1964). Furthermore, reequilibration processes are known to occur during cooling and metamorphism (Buddington and Lindsley 1964). Because the in-situ analyses from this study were intentionally located to avoid large exsolution microtextures, the magnetite samples analyzed have compositions that are likely not representative of their primary magmatic composition and hence have affected their positions on these discrimination diagrams. Second, the data used to generate the Dupuis and Beaudoin (2011) diagrams does not include data from magnetite-dominated Proterozoic massif-type anorthosite hosted Fe-Ti-V deposits. For this reason, magnetite from the present study does not plot within the Fe-Ti, V oxide field. As such, the Fe-Ti, V oxide field needs to be modified in the Dupuis and Beaudoin (2011) diagram, or bulk analyses of magnetite mineral separates are required in order to rehomogenize microscopic and macroscopic exsolution features to better constrain magmatic magnetite composition (Charlier et al. 2009)

In addition to XY discrimination diagrams, Dare et al. (2014) proposed a multi-element empirical discrimination diagram for magnetite. On these diagrams, magnetite data are normalized to bulk continental crust values (Fig. 11). Because the trace element composition of magnetite is thought to reflect the composition of the melt or fluid from which it crystallized, discrimination fields for magnetite from magmatic Fe-Ti-V deposits (primitive magnetite), Fe-Ti-P deposits (evolved magnetite), high-T hydrothermal deposits, felsic plutons, and andesite were proposed to have different patterns on the diagram. For the purpose of the present study, only the high-T hydrothermal

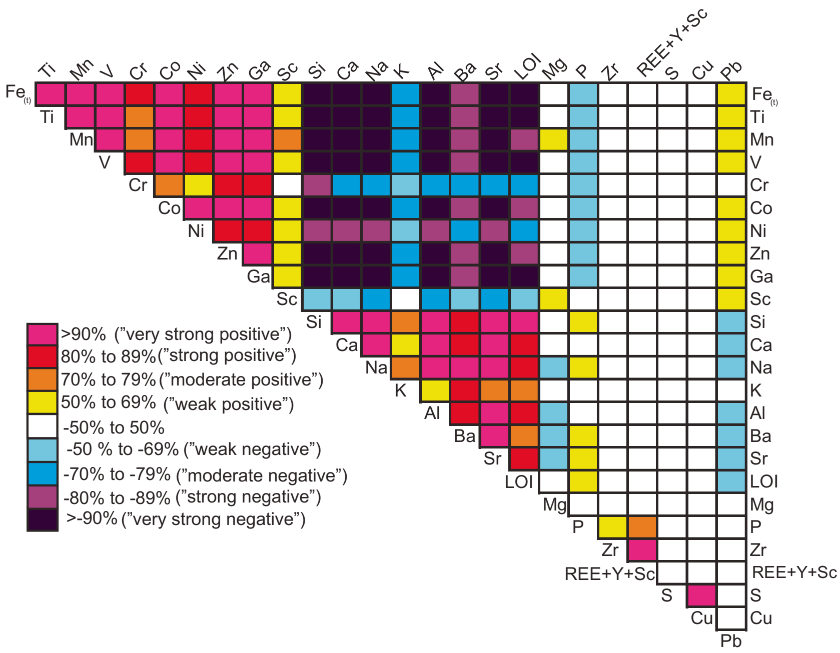

Fig. 6 Correlation matrix of elements from whole-rock analyses. Positive correlations are present between all elements associated with Fe-Ti oxide minerals (Fe, Ti, Mn, Cr, Co, Ni, Zn, Ga, and Sc), as well as between all elements associated with plagioclase (Si, Ca, Na, K, Al, Ba, Sr, and LOI). Elements associated with Fe-Ti oxide mineralization are negatively correlated with elements associated with plagioclase. Phosphorus, which is correlated to the presence of apatite, is weakly positively correlated with plagioclase associated elements and weakly negatively associated with elements associated with Fe-Ti oxide minerals

magnetite and magmatic Fe-Ti-V oxide patterns were used because those fields most closely match proposed models for genesis of Fe-Ti oxide mineralization in Proterozoic massif-type anorthosites (Charlier and Grove 2012). The high-T hydrothermal and magmatic Fe-Ti-V magnetite fields overlap in the majority of the elements measured in the present study. Complete overlap occurs with Si, Y, P, Ta, Nb, Cu, Mo, Sn, Ga, Mn, Zn, and Co, and partial overlap occurs in Ca, Ge, and W, so the latter elements are not useful for discrimination purposes. Only Pb, Zr,

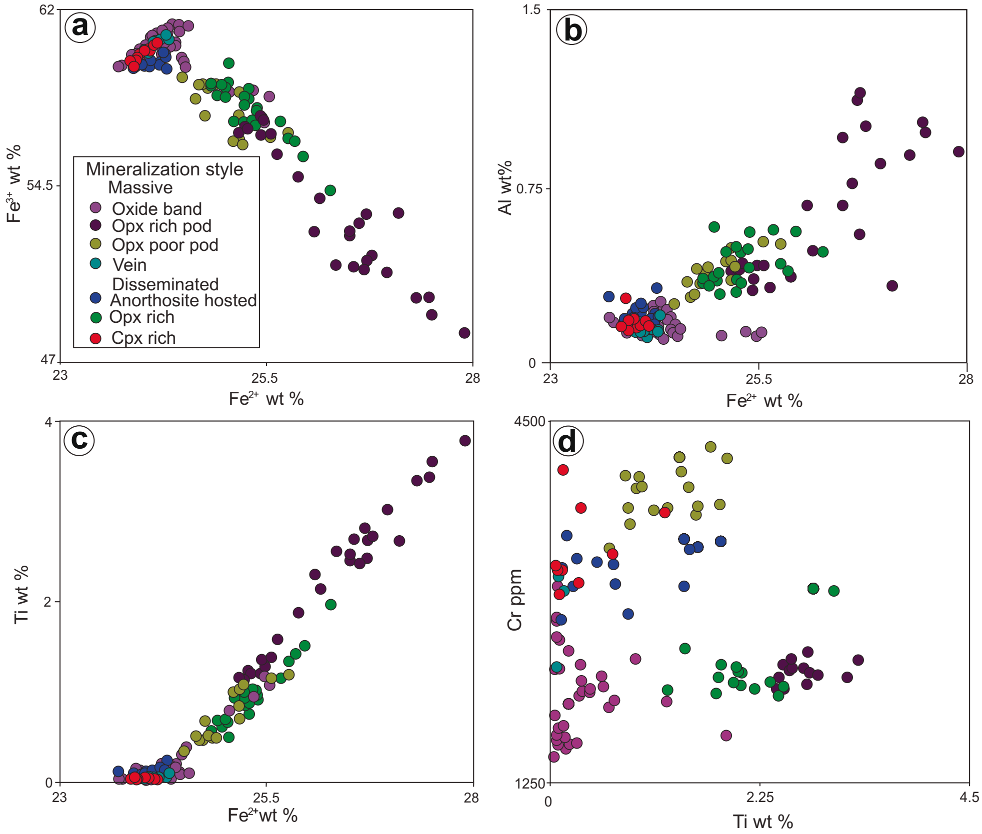

Fig. 7 Binary element variation diagrams of magnetite analyses. **a** Negative correlation between Fe^{2+} and Fe^{3+}. **b** Positive correlation between Fe^{2+} and Ti suggesting varying amounts of ilmenite exsolution. **c** Positive correlation between Fe^{2+} and Al suggesting varying amounts of pleonaste exsolution. **d** Lack of correlation between Cr and Ti; both being highly compatible elements in magnetite, which suggest a loss of primary magmatic composition of magnetite

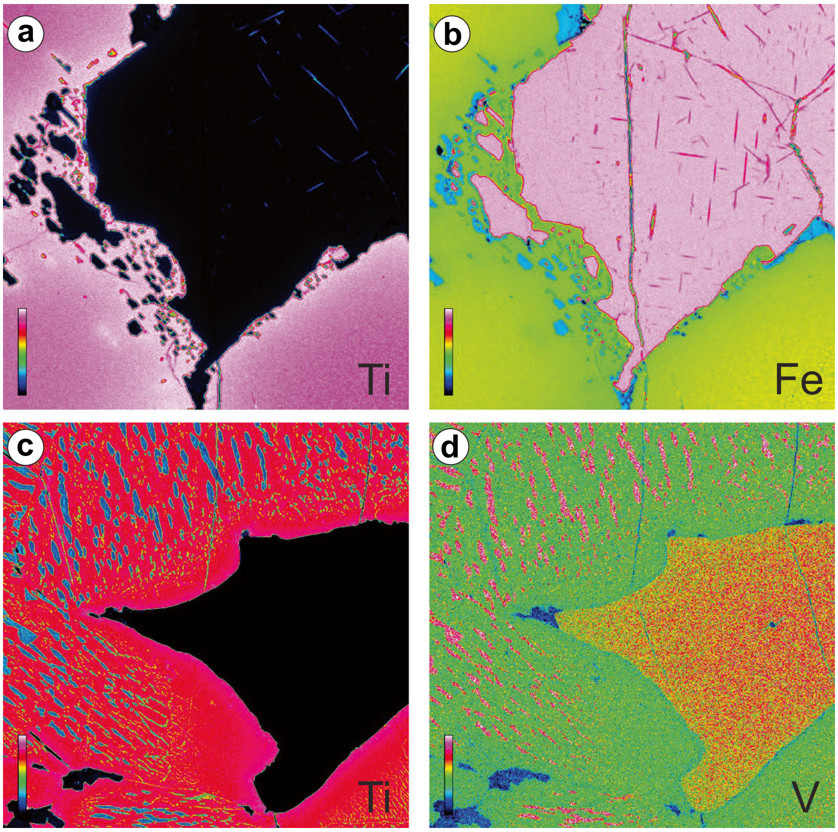

Fig. 8 Representative semi-quantitative EPMA WDS X-ray maps of magnetite, ilmenite, and pleonaste from selected mineralized samples. Maps have a relative "temperature" scale with the warmest colors representing the highest abundance of the element in question. **a** Ti content variations at the contact between magnetite and ilmenite; note high Ti rim in ilmenite (pink in color) at contact with magnetite and lamellae in magnetite slightly enriched in Ti. **b** Map showing variation in Fe content from the area analyzed in **a**. Note zone of low Fe at contact between magnetite (pink) and ilmenite (yellow). Dark pink lenses in magnetite correspond with pleonaste exsolution features as observed with transmitted light microscopy. **c** WDS map of Ti content variation at contact between ilmenite and magnetite. As in **a**, a high Ti rim is present in ilmenite (red) immediately adjacent to contact between magnetite (black) and ilmenite. Note low Ti lenses in ilmenite correspond with hematite as observed with reflected light microscopy. **d** V content variation from the area analyzed in **c**. Note slight enrichment in V content in core of magnetite grain vs rim and enriched V content in hematite lenses in ilmenite

Hf, Al, Ti, V, Ni, and Cr do not have any overlap, so these elements are the most useful for discriminating between magmatic and high-T hydrothermal magnetite; however, the geochemical rationale for why these elements work to discriminate different magnetite types needs to be more adequately explained. Moreover, regardless of the mineralization style, data from the present study did not consistently plot uniquely in either field (Fig. 11), and the lack of clear affinity with either of the fields is also illustrated on Fig. 12. These results indicate that even magnetite analyses from a known deposit style do not plot correctly on these diagrams.

Effect of cooling and metamorphism on oxide chemistry

Fe-Ti oxide minerals are known to experience extensive subsolidus reequilibration during periods of slow cooling, as well as during metamorphism (Buddington and Lindsley 1964; Duchesne 1970; Lindsley 1991). The net effect of reequilibration is purification of the oxide minerals towards their end-member stoichiometric compositions by means of exsolution, oxide-oxide reequilibration, and oxide-silicate reequilibration (Buddington and Lindsley 1964).

The presence of abundant and complex exsolution features in oxide minerals in the NWRA suggests that the in-situ oxide analyses are not representative of primary magmatic compositions; rather, they are representative of the point at which exsolution and inter-oxide reequilibration ceased. Microtextures composed of pleonaste and ilmenite in magnetite, as well as granular ilmenite and pleonaste adjacent to magnetite, suggest that primary magmatic magnetite contained higher concentrations of Ti, Al, and Mg compared with the magnetite analyzed. Likewise, the presence of hematite lenses, spinel lamellae, and magnetite lamellae in ilmenite suggests that the coarsest-grained

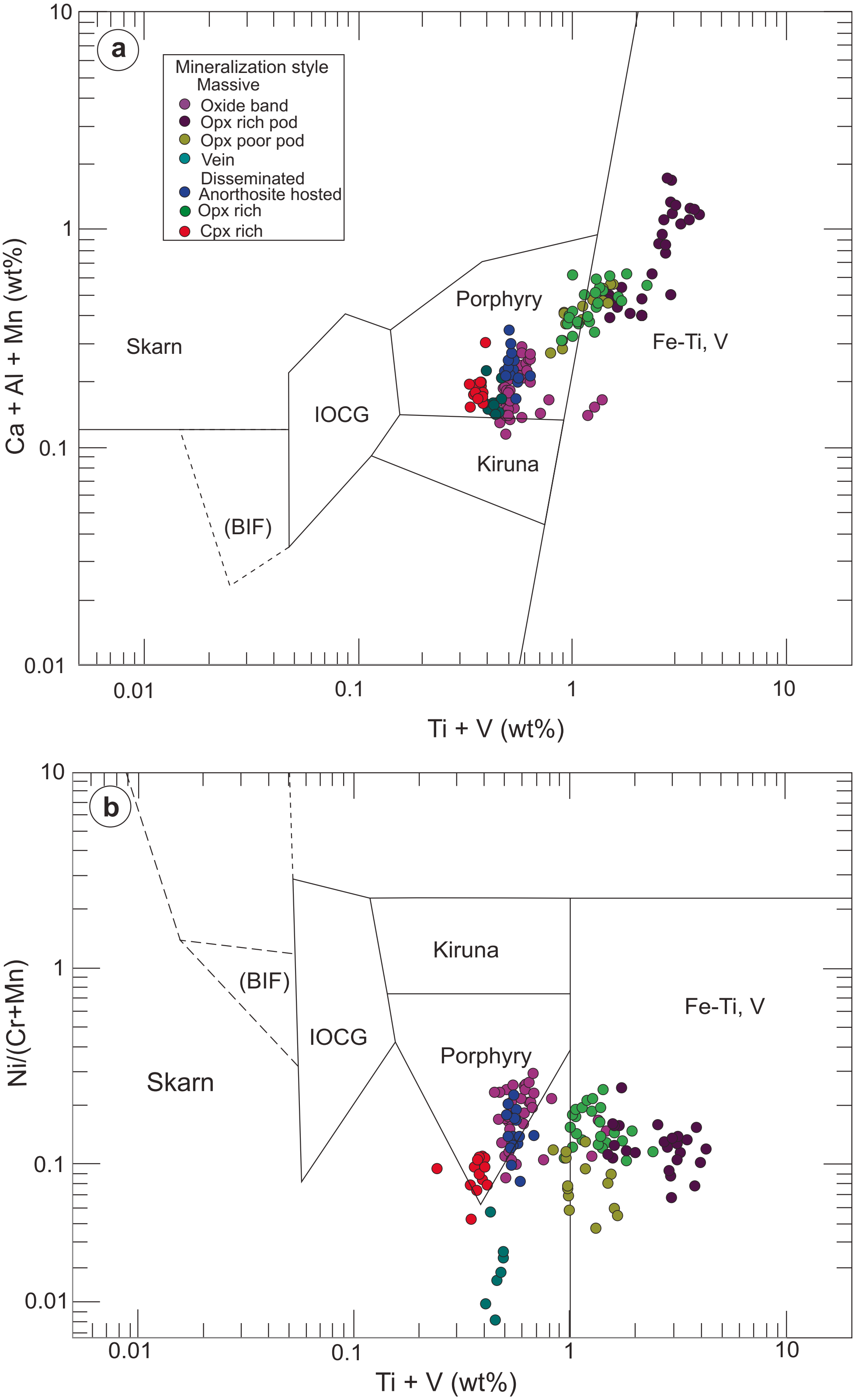

Fig. 9 Magnetite ore deposit discrimination diagrams of Dupuis and Beaudoin (2011). **a** Diagram using Ca + Al + Mn (wt%) as the Y axis and Ti + V (wt%) as the X axis. **b** Diagram using Ni/(Cr + Mn) as the Y axis and Ti + V (wt%) as the X axis. Magnetite analyses from this study were plotted on the diagram. See text for details

exsolved ilmenite had a higher hematite component, as well as higher Mg and Al contents compared with the analyzed ilmenite. Inter-oxide reequilibration is also responsible for oxide purification. For example, adjacent Ti-magnetite and ilmenite interact following the reaction $FeTi_2O_4$ (in magnetite) + Fe_2O_3 (in ilmenite) → Fe_3O_4 (in

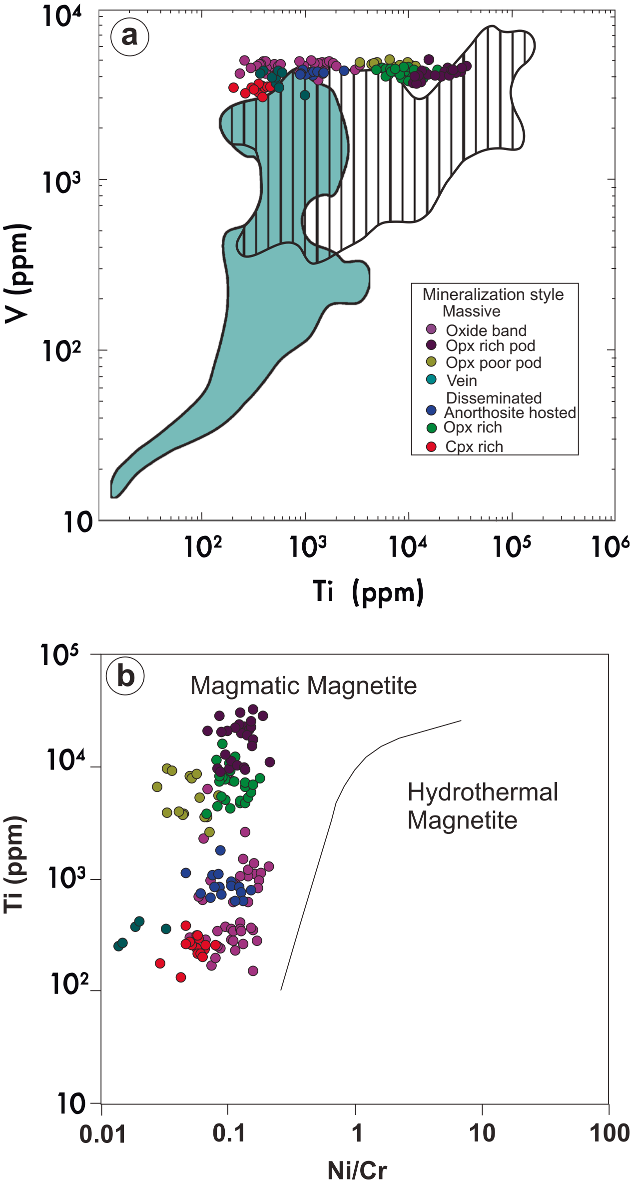

Fig. 10 **a** Hydrothermal vs magmatic discrimination diagram proposed by Knipping et al. (2015) using Ti as the X axis and V for the Y axis. The diagram contains three fields; a magmatic magnetite field (vertical lines), a hydrothermal magnetite field (teal field), and a magmatic-hydrothermal magnetite field (vertical lines on a teal field). Most coarse-grained magnetite data from this study plot above all fields of the discrimination diagram due to its high V content. **b** Hydrothermal vs magmatic discrimination diagram proposed by Dare et al. (2014) using Ni/Cr as the X axis and Ti (ppm) as the Y axis. All magnetite analyses, regardless of mineralization style, plot in the magmatic field

magnetite) + $FeTiO_3$ (in ilmenite) resulting in pure end member magnetite and ilmenite (Buddington and Lindsley 1964; Duchesne 1972).

Oxide minerals in the NWRA underwent two periods of reequilibration: (1) during autometamorphism caused by the residual heat of the host anorthosite coupled with slow cooling (Duchesne 1972; Morisset et al. 2010) and (2) during overprinting during Grenvillian metamorphism (Rivers 2008, 2015). It is difficult to differentiate which exsolution features are associated with autometamorphism and which are associated with overprinting Grenvillian metamorphism, as the grade of Grenvillian metamorphism has not been well constrained within the NWRA. According to Rivers (2008), the NWRA is located within the Grenvillian orogenic lid, which is thought to have reached a maximum temperature of ~650 °C. As coarse-grained granular exsolution features, as well as pleonaste exsolution in magnetite, occur at >750 °C (Buddington and Lindsley 1964; Mücke 2003), those features are likely autometamorphic features that formed during anorthosite cooling. In contrast, ülvospinel can exsolve from magnetite down to ~600 °C (Buddington and Lindsley 1964). Further, ülvospinel exsolution can be subsequently oxidized to ilmenite over a wide range of temperatures (Buddington and Lindsley 1964). This suggests that finer-grained ilmenite exsolution within and adjacent to coarse-grained magnetite formed at lower temperatures, possibly during anorthosite cooling as well as during Grenvillian metamorphism. The combined effects of autometamorphism and Grenvillian metamorphism significantly modified the primary Fe-Ti oxide compositions.

Recent studies of Fe-Ti oxide mineralization (e.g., Charlier et al. 2009, 2010) suggest that analyzing oxide mineral separates results in a more accurate representation of true magmatic oxide compositions. Re-integration of exsolution features into the host magnetite using relative abundances of exsolution features coupled with in-situ analyses of each type of exsolution feature observed has been used in the past (e.g., Bowles 1977; Pang et al. 2008). However, these approaches are likely flawed because they cannot accurately constrain inter-oxide reequilibration, oxide-silicate reequilibration, reequilibration between oxide minerals and trapped liquid, or the presence and amount of external granule exsolution, wherein ilmenite and pleonaste granules form at the grain boundaries of magnetite during subsolidus conditions (Buddington and Lindsley 1964; Duchesne 1972; Charlier et al. 2009).

The relative proportions of primary oxides and those formed through external granule exsolution in the NWRA are unclear. However, the following observations suggest that ilmenite and pleonaste made up only minor components of the primary magmatic oxide mineral assemblage, and the ilmenite and pleonaste granules are instead the product of external granule exsolution based on: (1) in the massive oxide mineralization, the magnetite is coarser-grained than granular ilmenite and pleonaste; (2) in the massive oxide mineralization, the coarsest ilmenite and pleonaste are spatially associated with each other and occur in clusters; (3) zones enriched in ilmenite or pleonaste relative to magnetite are not observed in either the massive to semi-massive mineralization or disseminated oxide mineralization; (4) no primary pleonaste or ilmenite is observed associated with the disseminated oxide

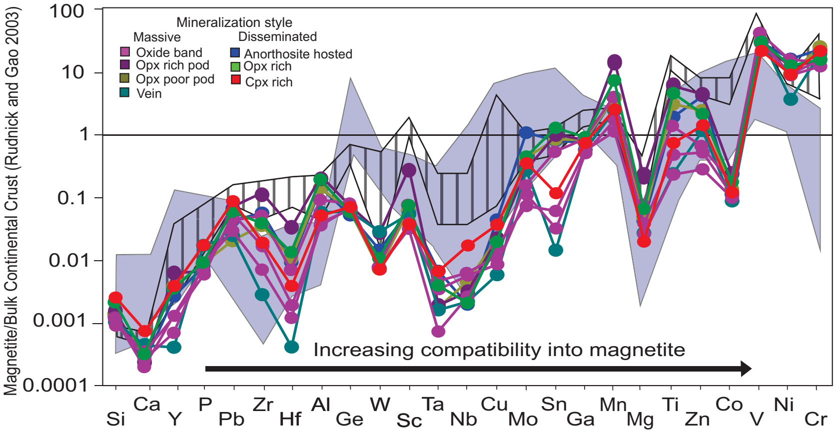

Fig. 11 Discrimination diagram for trace element LA-ICP-MS analyses proposed by Dare et al. (2014). The trace element composition of magnetite is normalized to bulk continental crust of Rudnick and Gao (2003) and organized in order of compatibility in magnetite. Discriminant fields for Fe-Ti-V magmatic magnetite (vertical stripes) and high-T hydrothermal magnetite (periwinkle) are plotted. Data from this study were averaged and plotted on separate figures by mineralization style as labeled on each diagram

mineralization; and (5) no disseminated mineralization that is dominated by ilmenite or pleonaste is observed. Similar conclusions are drawn to explain the presence of magnetite-dominated ilmenite-bearing Fe-Ti oxide mineralization hosted in the Late Permian Panzhihua-layered gabbro intrusion of southwest China (Pang et al. 2008). Because external granule exsolution

Fig. 12 Companion figure to Fig. 11 showing the plotting area of magnetite analyses from various mineralization styles. Red squares represent points plotting within the magmatic magnetite field, blue squares represent points plotting within the hydrothermal field, purple squares represent points plotting in the overlap between magmatic and hydrothermal fields, and white squares represent points plotting outside of any field

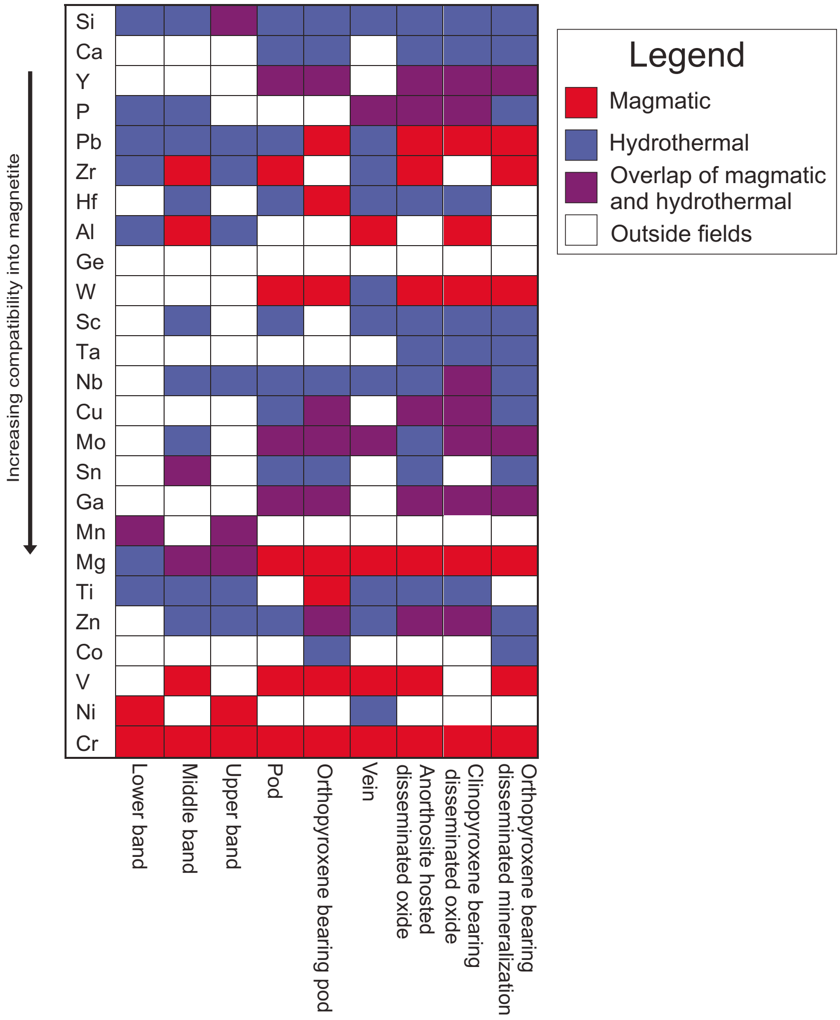

	Lower band	Middle band	Upper band	Pod	Orthopyroxene bearing pod	Vein	Anorthosite hosted disseminated oxide	Clinopyroxene bearing disseminated oxide	Orthopyroxene bearing disseminated mineralization
Si	🟦	🟦	🟪	🟦	🟦	🟦	🟦	🟦	🟦
Ca	⬜	⬜	⬜	🟦	🟦	⬜	🟦	🟦	🟦
Y	⬜	⬜	⬜	🟪	🟪	⬜	🟪	🟪	🟪
P	🟦	🟦	⬜	⬜	⬜	🟪	🟪	🟪	🟦
Pb	🟦	🟦	🟦	🟦	🟥	🟦	🟥	🟥	🟥
Zr	🟦	🟥	🟦	🟥	⬜	🟦	🟥	⬜	🟥
Hf	⬜	🟦	⬜	🟦	🟥	🟦	🟦	🟦	⬜
Al	🟦	🟥	🟦	⬜	⬜	🟥	⬜	🟥	⬜
Ge	⬜	⬜	⬜	⬜	⬜	⬜	⬜	⬜	⬜
W	⬜	⬜	⬜	🟥	🟥	🟦	🟥	🟥	🟥
Sc	⬜	🟦	⬜	🟦	⬜	🟦	🟦	🟦	🟦
Ta	⬜	⬜	⬜	⬜	⬜	⬜	🟦	🟦	🟦
Nb	⬜	🟦	🟦	🟦	🟦	🟦	🟦	🟪	🟦
Cu	⬜	⬜	⬜	🟦	🟪	⬜	🟪	🟪	🟦
Mo	⬜	🟦	⬜	🟪	🟪	🟪	🟦	🟪	🟪
Sn	⬜	🟪	⬜	🟦	🟦	⬜	🟦	⬜	🟦
Ga	⬜	⬜	⬜	🟪	🟪	⬜	🟪	🟪	🟪
Mn	🟪	⬜	🟪	⬜	⬜	⬜	⬜	⬜	⬜
Mg	🟦	🟪	🟪	🟥	🟥	🟥	🟥	🟥	🟥
Ti	🟦	🟦	🟦	⬜	🟥	🟦	🟦	🟦	⬜
Zn	⬜	🟦	🟦	🟦	🟪	🟦	🟪	🟪	🟦
Co	⬜	⬜	⬜	⬜	🟦	⬜	⬜	⬜	🟦
V	⬜	🟥	⬜	🟥	🟥	🟥	🟥	⬜	🟥
Ni	🟥	⬜	🟥	⬜	⬜	🟦	⬜	⬜	⬜
Cr	🟥	🟥	🟥	🟥	🟥	🟥	🟥	🟥	🟥

occurs at such high temperatures (between 600 and < 880 °C; Buddington and Lindsley 1964), the exsolution product itself will be impure and upon cooling will contain exsolution features, as are observed in coarse granular ilmenite and pleonaste in the NWRA.

Origin and evolution of Fe-Ti oxide mineralization in the NWRA

Fe-Ti oxide mineralization in the NWRA shows evidence of a three-step formation process: (1) late-stage magmatic crystallization of primary, chemically-impure magnetite; (2) concentration of Fe-Ti oxide minerals by solid-state remobilization; and (3) reequilibration during subsequent post-emplacement cooling and subsequent autometamorphism and Grenvillian metamorphism. Evidence of the process responsible for the primary ore genesis of the oxide mineralization has largely been obliterated during recrystallization of oxides and host anorthosite, oxide remobilization, and subsolidus exsolution and reequilibration of the oxide minerals.

The original formation process of the Fe-Ti oxide mineralization must be able to explain the presence of significant quantities of primary, chemically-impure magnetite, as well as both orthopyroxene-bearing and orthopyroxene-poor oxide mineralization. Either magma mixing (Irvine 1977; Charlier et al. 2010) or fractional crystallization of a Fe-Ti-P-bearing mafic silicate magma (Charlier et al. 2006, 2007, 2008) may have been responsible for the genesis of the oxide mineralization. However, little evidence for either process is preserved in the oxide minerals due to extensive reequilibration of the oxide minerals, which obliterated both the primary compositions and textures of the oxides.

During emplacement of the anorthosite suite, two processes are invoked to concentrate the oxide minerals: (1) differential stress on the rigid host anorthosite causes the more ductile Fe-Ti oxide minerals to concentrate in zones of low pressure in the less ductile anorthosite via diffusion creep, a process also known as solid-state remobilization (Duchesne 1996, 1999); or (2) density-based crystal sorting concentrates Fe-Ti oxide mineralization (Pang et al. 2008). Either process could create zones of pure mono-mineralic Ti-, Al-, and Mg-bearing magnetite; however, several lines of evidence suggest that the oxides were concentrated via solid-state remobilization. A key observation presented by Pang et al. (2008) in support of their density-based crystal sorting model is gradational contacts between host-rock and massive oxide mineralization; these contact relationships are not observed in the NWRA. Furthermore, the presence of oxides rimming pyroxene in the host-rock, the fact that oxide minerals are interstitial to plagioclase in the host anorthosite, and the irregular nature of the contacts between oxide minerals and host-rocks suggest that crystal settling is not viable for the NWRA and that solid-state remobilization was the primary oxide concentrating process. Finally, it is also likely that the massive mono-mineralic magnetite cooled and presumably began to exsolve and reequilibrate to form the textures presently observed. At the highest temperatures, coarse granules of pleonaste and ilmenite were formed at grain boundaries of magnetite followed by all other textures of pleonaste, magnetite, and ilmenite exsolution (Buddington and Lindsley 1964; Duchesne 1970). The long period of slow cooling coupled with Grenvillian metamorphism resulted in the coarse- to very coarse-grained nature of the oxide mineralization as well as the near end-member concentrations of magnetite and ilmenite (Buddington and Lindsley 1964; Charlier et al. 2015).

Economic significance

The magnetite-ilmenite present in the NWRA, while limited in areal extent, is similar to other types of massif-type anorthosite-hosted mineralization globally (e.g., Charlier and Grove 2012). Moreover, our integrated field, textural, and micro-analytical approach to understanding the origin and complexity of magnetite-ilmenite formation in the NWRA is an approach that is applicable to any magnetite-ilmenite-bearing deposit-type globally, be it massif-type anorthosite-hosted Fe-Ti-V mineralization, IOCG, or porphyry Cu-Au. Our results clearly illustrate that the origin of the chemical variation and processes of magnetite-(ilmenite) formation are quite complex, involving magmatic crystallization and subsolidus requilibration, diffusion, and chemical and mineralogical re-organization. This should be considered the norm, rather than the exception, and is something that must be considered whenever evaluating the origins of anorthosite-hosted Fe-Ti-V mineralization and the composition of the minerals present within said mineralization.

The complexity of chemical processes and requilibration in anorthosite-hosted mineralization is also recorded in the various magnetite discrimination diagrams utilized to discriminate magnetite from different mineral deposit types. In particular, our results show that many published discrimination diagrams are not effective at determining the origin of the analyzed magnetite in massif-type anorthosites, and using such empirical discrimination diagrams is problematic for the discrimination of certain mineral deposit types that have complex petrogenetic and/or hydrothermal origins. Similarly, using these diagrams for unknown magnetite grains (e.g., magnetite found in heavy mineral concentrates from surficial materials) is also problematic and could lead to erroneous deposit-type classifications and by consequence erroneous exploration strategies if magnetite chemistry is the sole basis upon which an exploration program has been constructed. Thus, additional features beyond magnetite chemistry (e.g., geology, geochemistry, mineral assemblages, other mineral phase chemistry, paleotectonic setting) must also be used to discriminate a deposit type so as to ensure that magnetite chemistry is only part of a broader, more robust exploration strategy.

Conclusions

The Fe-Ti oxide mineralization in the NWRA is coarse-grained and magnetite-dominated, containing minor amounts of ilmenite and pleonaste. The Fe-Ti oxide mineralization is present in zones of massive to semi-massive oxide mineralization and as disseminated oxide mineralization. The Fe-Ti oxide mineralization is in sharp, irregular, contact with the host anorthosite. No textural or in-situ chemical variation is observed between mineralization styles. Subsolidus processes including exsolution and reequilibration that occurred during slow cooling of the host anorthosite body coupled with Grenvillian metamorphism have significantly modified the magnetite ilmenite and pleonaste chemical compositions, and primary magmatic oxide compositions are not preserved. Instead, the analyses are representative of post-reequilibration oxide compositions. It is clear that subsolidus processes occurred both during the post-emplacement period and in response to Grenvillian metamorphism. However, the extent of the subsolidus processes during each event is unclear.

EPMA and LA-ICPMS-based empirical magnetite discrimination diagrams illustrate that the NWRA Proterozoic massif-type anorthosite-hosted magnetite analyses do not plot exclusively in the expected Fe-Ti-V fields. It is possible that the Ti and Al contents and other trace elements in magnetite were significantly modified during subsolidus exsolution of ilmenite and pleonaste, respectively, as well as during reequilibration leading to erroneous discrimination. This suggests that care must be taken using these diagrams on magnetite from Proterozoic massif-type anorthosites that have undergone prolonged crystallization histories or have been affected by thermal reequilibration during deformation and metamorphism.

The formation and evolution of Fe-Ti oxide mineralization in the NWRA occurred through three distinct processes: (1) late-stage magmatic crystallization of primitive, chemically impure magnetite; (2) concentration by solid-state remobilization or crystal sorting; and (3) reequilibration during subsequent post-emplacement cooling and subsequent autometamorphism and Grenvillian metamorphism.

Acknowledgements Tom Benoit and Craig Coady of Ferrum Resources are thanked for providing permission to undertake this study on the Cape Caribou, Labrador property and for field and logistics assistance. Andy Kerr and James Conliffe are thanked for their support, encouragement, and advice during the project. Danny Savard and Brian Joy are thanked for assistance with in-situ LA-ICPMS and EPMA analyses, respectively. Lastly, thanks to Editor Bernd Lehmann, Associate Editor Wolfgang Meier, and an anonymous reviewer for their constructive comments that greatly improved this manuscript.

Funding information This project is supported by funds from the Ignite R&D Program of the Research and Development Corporation (RDC) of Newfoundland and Labrador, the Atlantic Canada Opportunities Agency (ACOA), and Innovation, Business, and Rural Development (IBRD) to M.L.D. Fonkwe. Travel for the second field season was funded by the Northern Scientific Training Program (NSTP). SJP's research is funded by an NSERC Discovery Grant, and this study was also supported by the NSERC-Altius Industrial Research Chair in Mineral Deposits funded by NSERC, Altius Resources Inc., and RDC.

References

Ashwal LD (1982) Mineralogy of mafic and Fe-Ti oxide-rich differentiates of the Marcy anorthosite massif, Adirondacks, New York. Am Mineral 67:14–27

Ashwal LD (1993) Anorthosites. Spinger-Verlag, Berlin, p 422

Ashwal LD (2010) The temporality of anorthosites. Can Mineral 48:711–728

Augland LE, Moukhsil A, Solgadi F, Indares A (2015) Pinwarian to Grenvillian magmatic evolution in the central Grenville Province: new constraints from ID-TIMS U-Pb ages and coupled Lu-Hf S-MC-ICP-MS data. Can J Earth Sci 52:701–721

Bowles JF (1977) A method of tracing the temperature and oxygen-fugacity histories of complex magnetite-ilmenite grains. Mineral Mag 41:103–109

Broughm SG, Hanchar JM, Tornos F, Westhaus A, Attersley S (2017) Mineral chemistry of magnetite from magnetite-apatite mineralization and their host rocks: examples from Kiruna, Sweden and El Laco, Chile. Mineralium Deposita 52:1223–1244

Buddington AF, Lindsley DH (1964) Iron-titanium oxide minerals and synthetic equivalents. J Petrol 5:310–357

Bussy F, Krogh T, Wardle RJ (1995) Late Labradorian metamorphism and anorthosite-granitoid intrusion, Cape Caribou River Allochthon, Grenville Province, Labrador: evidence from U-Pb geochronology. Can J Earth Sci 32:1411–1425

Butt JM (2000) Mineral chemistry and mineral reactions in a meta-anorthosite complex, Cape Caribou River Allochthon, Grenville Province, Labrador. Unpublished B.Sc. Thesis, Memorial University of Newfoundland, St. John's NL, 111 pp.

Charlier B, Grove TL (2012) Experiments on liquid immiscibility along tholeiitic liquid lines of descent. Contrib Mineral Petrol 164:27–44

Charlier B, Duchesne JC, Vander Auwera J (2006) Magma chamber processes in the Tellnes ilmenite deposit (Rogaland Anorthosite Province, SW Norway) and the formation of Fe-Ti ores in massif type anorthosites. Chem Geol 234:264–290

Charlier B, Skår Ø, Korneliussen A, Duchesne JC, Vander Auwera J (2007) Ilmenite composition in the Tellnes Fe–Ti deposit, SW Norway: fractional crystallization, postcumulus evolution and ilmenite–zircon relation. Contrib Mineral Petrol 154:119–134

Charlier B, Sakoma E, Sauvé M, Stanaway K, Vander Auwera J, Duchesne JC (2008) The grader layered intrusion (Havre-Saint-Pierre Anorthosite, Quebec) and genesis of nelsonite and other Fe–Ti–P ores. Lithos 101:359–378

Charlier B, Namur O, Duchesne JC, Wisniewska J, Parecki A, Vander Auwera J (2009) Cumulate origin and polybaric crystallization of Fe-Ti oxide ores in the Suwalki anorthosite, NE Poland. Econ Geol 104:205–221

Charlier B, Namur O, Malpas S, de Marneffe C, Duschene JC, Vander Auwera J, Bolle O (2010) Origin of the giant Allard Lake ilmenite ore deposit (Canada) by fractional crystallization, multiple magma pulses and mixing. Lithos 117:119–134

Charlier B, Namur O, Bolle O, Latypov R, Duchesne JC (2015) Fe-Ti-V-P ore deposits associated with Proterozoic massif-type anorthosites and related rocks. Earth Sci Rev 141:56–81

Chen WT, Zhou MF, Zhao TP (2013) Differentiation of nelsonitic magmas in the formation of the ~1.74 Ga Damiao Fe-Ti-P ore deposit, North China. Contrib Mineral Petrol 165:1342–1362

Dare SAS, Barnes SJ, Beaudoin G (2012) Variation in trace element content of magnetite crystallized from a fractionating sulfide liquid, Sudbury, Canada: implications for provenance discrimination. Geochim Cosmochim Acta 88:27–50

Dare SA, Barnes SJ, Beaudoin G, Meric J, Boutroy E, Potvin-Doucet C (2014) Trace elements in magnetite as petrogenetic indicators. Mineral Deposita 49:785–796

Dill HG (2010) The "chessboard" classification scheme of mineral deposits: mineralogy and geology from aluminum to zirconium. Earth Sci Rev 100:1–420

Duchesne JC (1970) Microtextures of Fe-Ti oxide minerals in the South Rogaland anorthositic complex (Norway). Ann Soc Geol Belg 93: 197–251

Duchesne JC (1972) Iron-titanium oxide minerals in the Bjerkrem-Sogndal Massif, southwestern Norway. J Petrol 13:57–81

Duchesne JC (1996) Liquid ilmenite or liquidus ilmenite: a comment on the nature of ilmenite vein deposits. In: Demaiffe D (ed) Petrology and geochemistry of magmatic suites of rocks in the continental and oceanic crusts. A volume dedicated to Professor Jean Michot, Tervuren, pp 73–82

Duchesne JC (1999) Fe-Ti deposits in Rogaland anorthosites (South Norway): geochemical characteristics and problems of interpretation. Mineral Deposita 34:182–198

Dupuis C, Beaudoin G (2011) Discriminant diagrams for iron oxide trace element fingerprinting of mineral deposit types. Mineral Deposita 36:319–355

Dyke B, Kerr A, Sylvester PJ (2004) Magmatic sulfide mineralization at the Fraser Lake prospect (NTS Map Area 13L/5), Michikamau Intrusion, Labrador. Current Research, Newfoundland and Labrador Geological Survey, Report 04: 7–22

Dymek RF, Owens BE (2001) Petrogenesis of apatite rich rocks (nelsonites and oxide-apatite gabbronorites) associated with massif anorthosites. Econ Geol 96:797–815

Fabjan C, Garche J, Harrer B, Kolbeck C, Philippi F, Tomazic G, Wagner F (2001) The vanadium redox-battery: an efficient storage unit for photovoltaic systems. Electrochim Acta 47:825–831

Force ER (1991) Geology of titanium-mineral deposits. Geol Soc Am Spec Pap 259:112

Gower CF (1996) The evolution of the Grenville Province in Eastern Labrador, Canada. Geol Soc Lond Spec Publ 112:197–218

Gower CF, Krogh TE (2002) A U-Pb geochronological review of the Proterozoic history of the eastern Grenville Province. Can J Earth Sci 39:795–829

Gower CF, Schärer U, Heaman LM (1992) The Labradorian orogeny in the Grenville Province, eastern Labrador. Can J Earth Sci 29:1944–1957

Gower CW, Kamo SL, Kwok K, Krogh TE (2008) Proterozoic southward accretion and Grenvillian orogenesis in the interior Grenville Province in eastern Labrador: evidence from U–Pb geochronological investigations. Precambrian Res 165(1–2):61–95

Hinchey JG (1999) Magmatic sulphide-oxide mineralization in the Nain area, northern Labrador: a petrological and geochemical study. Unpublished B.Sc. Thesis, Memorial University, St. John's, NL, 131 pp.

Hitzman MW, Oreskes N, Einaudi MT (1992) Geological characteristics and tectonic setting of Proterozoic iron oxide (Cu-U-Au-REE) deposits. Precambrian Res 58:241–287

Hu H, Li JW, Lentz D, Ren Z, Zhao XF, Deng XD, Hall D (2014) Dissolution-reprecipitation process of magnetite from the Chengchao iron deposit: insights into ore genesis and implication for in-situ chemical analysis of magnetite. Ore Geol Rev 57:393–405

Jochum KP, Willbold M, Raczek I, Stoll B, Herwig K (2005) Chemical characterization of the USGS reference glasses GSA-1G, GSC-1g, GSD-1g, GSE-1g, BCR-2G, BHVO-2G, and BIR-1G using EPMA, ID-TIMS, ID-ICP-MS and LA-ICPMS. Geostand Geoanal Res 29: 285–302

Kerr A, Macdonald HE, Naldrett AJ (2001) Geochemistry of the Pants Lake Intrusion, Labrador: implications for future mineral exploration. Newfoundland and Labrador Department of Mines and Energy, Mineral Resource Report 2001:191–228

Kerr A, Walsh JA, Sparkes GW, Hinchey JG (2013) Vanadium potential in Newfoundland and Labrador: a review and assessment. Newfoundland and Labrador Department of Natural Resources, Geological Survey 13:137–165

Knipping JL, Bilenker LD, Simon AC, Reich M, Barra F, Deditus AP, Walle M, Heinrich CA, Holtz F, Munizaga R (2015) Trace elements in magnetite from massive iron oxide-apatite deposits indicate a combined formation by igneous and magmatic-hydrothermal processes. Geochim Cosmochim Acta 171:15–38

Krauss JB (2002) High-pressure (HP), granulite-facies thrusting in a thick-skinned thrust system in the eastern Grenville Province, central Labrador. Unpublished M.Sc. Thesis, Memorial University of Newfoundland, St. John's NL, 377 pp.

Krauss JB, Rivers T (2004) High pressure granulites in the Grenvillian Grand Lake Thrust System, Labrador: pressure-temperature conditions and tectonic evolution In: Tollo RP, McLelland J, Corriveau L, Bartholomew MJ (eds) Proterozoic tectonic evolution of the Grenville orogen in North America: Geological Society of America Memoir 197:105–134

Li ZX, Bogdanova SV, Collins AS, Davidson A, De Waele B, Ernst RE, Fitzsimons ICW, Fuck RA, Gladkochub DP, Jacobs J, Karlstrom KE, Lu S, Natapov LM, Pease V, Pisarevsky SA, Thrane K, Vernikovsky V (2008) Assembly, configuration, and break-up history of Rodinia: a synthesis. Precambrian Res 160:179–210

Li X, Zhang H, Mai Z, Hm Z, Vankelecom I (2011) Ion exchange menbranes for vanadium redox flow battery (VRB) applications. Energy Environ Sci 4:1147–1160

Lindsley DH (1976) The crystal chemistry and structure of oxide minerals as exemplified by the Fe-Ti oxides. In Oxide minerals. Mineralogical Society of America, Short Course Notes 3: L1-L6

Lindsley DH (1991) Experimental studies of oxide minerals. Rev Mineral Geochem 25:69–109

MacDonald HE (1999) The geology, petrography and geochemistry of gabbroic rocks of the Pants Lake Intrusive Suite on the Donner/Teck South Voisey's Bay Property, north-central Labrador, Canada Unpublished M.Sc. Thesis, University of Toronto, Toronto, Ontario, 176 pp.

Morisset CE, Scoates JS, Weis D (2010) Rutile-bearing ilmenite deposits associated with the Proterozoic Saint-Urbain and Lac Allard anorthosite massif, Grenville Province, Quebec. Can Mineral 44:821–849

Mücke A (2003) Magnetite, ilmenite and ulvite in rocks and ore deposits: petrography, microprobe analyses and genetic implications. Mineral Petrol 77:215–234

Nadoll P, Mauk JL, Leveille RA, Koenig AE (2015) Geochemistry of magnetite from porphyry Cu and skarn deposits in the southwestern United States. Mineral Deposita 50(4):493–515

Pang KN, Zhou MF, Lindsley D, Zhao D, Malpas J (2008) Origin of Fe-Ti oxide ores in mafic intrusions: evidence from the Panzhihua intrusion, SW China. J Petrol 49:295–313

Paton C, Hellstrom J, Paul B, Woodhead J, Hergt J (2011) Iolite: freeware for the visualization and processing of mass spectrometric data. J Anal At Spectrom 26:2508–2518

Philippe S, Wardle RJ, Scharer U (1993) Labradorian and Grenvillian crustal evolution of the Goose Bay Region, Labrador: new U-Pb geochronological constraints. Can J Earth Sci 30:2315–2327

Rivers T (1997) Lithotectonic elements of the Grenville Province: review and tectonic implications. Precambrian Res 86:117–154

Rivers T (2008) Assembly and preservation of lower, mid, and upper orogenic crust in the Grenville Province—implications for the evolution of large hot long-duration orogens. Precambrian Res 167(3–4):237–259

Rivers T (2015) Tectonic setting and evolution of the Grenville Orogen: an assessment of progress over the last 40 years. Geosci Can 42(1): 77–124

Rivers T, Culshaw NG, Hynes A, Indares A, Jamieson R, Martignole J (2012) The Grenville orogen—a post-Lithoprobe perspective. In: Percival JA, Cook FA, Clowes R (eds) Tectonic styles in Canada: the lithoprobe perspective. Geological Association of Canada Special Paper, St. John's, pp 97–236

Rudnick RL, Gao S (2003) Composition of the continental crust. Treatise on Geochemistry 3:1–64

Ryan B, Neale T, McGuire J (1982) Descriptive notes to accompany geological maps of the Grand Lake area, Labrador 13F/10, 11, 14, 15: St. John's, Newfoundland, Newfoundland and Labrador Department of Mines and Energy, Mineral Development Division Maps 82–64 to 82–67

Ryan B, Wardle RJ, Gower CF, Nunn GAG (1995) Nickel-copper-sulfide mineralization in Labrador: the Voisey's Bay discovery and its exploration implications. Current Research, Newfoundland and Labrador Geological Survey 95:177–204

Taner MF, Gault RA and Ercit, TS (2000) Vanadium mineralization and its industry in Canada. Geological Association of Canada, Mineral Deposits Division, The Gangue, Issue 65. Taner MF, Gault RA and Ercit, TS (2000) Vanadium mineralization and its industry in Canada. Geological Association of Canada, Mineral Deposits Division, The Gangue, Issue 65, p. 4–8

Valvasori A (2018) The origin and evolution of V-rich, magnetite dominated Fe-Ti oxide mineralization; Northwest River Anorthosite, south-central Labrador, Canada. Unpublished M.Sc. Thesis, Memorial University of Newfoundland, St. John's NL, 405 pp.

Wardle RJ, Ash C (1984) Geology of the Northwest River area. Current Research, Newfoundland Department of Mines and Energy, Mineral Development Division, Report 84: 53–67

Wardle RJ, Ash C (1986) Geology of the Goose Bay–Goose River area. Current Research, Newfoundland Department of Mines and Energy, Mineral Development Division, Report 86-1: 113–123

Wardle RJ, Ryan B, Philippe S, Scharer U (1990) Proterozoic crustal development, Goose Bay Region, Grenville Province, Labrador, Canada. In Gower, C.F., Rivers, T., Ryan, B. (eds) Mid-Proterozoic Laurentia-Baltica: Geological Association of Canada, Special Paper 38: 297–214

Wen G, Li JW, Hofstra AH, Koenig AE, Lowers HA, Adams D (2017) Hydrothermal reequilibration of igneous magnetite in altered granitic plutons and its implications for magnetite classification schemes: insights from the Handan-Xingtai Iron District, North China Craton. Geochim Cosmochim Acta 213:255–270